AN ABSTRACT OF THE THESIS OF

Kristina McCann-Grosvenor for the degree of Master of Science in Oceanography presented on December 10, 2010.

Title: Eddy Correlation Benthic O_2 Exchange Rates and Characterization of Sediment Properties from the Central Oregon Shelf at 30 Meters.

Abstract approved:

_____

Clare E. Reimers

Rates of benthic O_2 exchange are important measurements for determining organic matter remineralization, and can shed light on factors driving biogeochemical processes in coastal environments. Measurement of in situ O_2 consumption and production within permeable sediments, such as those found over ~43% of the Oregon-Washington shelf, has traditionally been done using methods that underestimate the flux for environments affected by waves.

Modified from atmospheric research, the non-invasive eddy correlation technique can measure O_2 flux across the sediment-water interface without disturbing the natural hydrodynamic flow. In 2009, eddy correlation measurements were made at discrete times over a 7-month period at a 30 m site off Yaquina Head, Newport, OR. The results of this newly developed method are evaluated here, together with properties of sediment cores taken at the study site. O_2 flux was found to be primarily into the bed (-6.2 to -30.7 mmol m^{-2} d^{-1}) and was enhanced during periods of higher bottom water O_2 concentration. Contributions to O_2 flux were seen in eddy correlation cospectra at surface wave frequencies and dependent on wave height. The sediments were fine sands with permeabilities of 1.3-4.7 x 10^{-11} m^2. Sediment pigment and organic carbon concentrations were low (chlorophyll-α : 0.03-0.45 μg g^{-1}, phaeophytin-α: 0.6-1.4 μg g^{-1} and organic carbon: 0.07-0.11 wt %), indicating high rates of organic matter export and/or remineralization. From these results it is inferred that physical forcing and changes in bottom water properties affect the inner shelf sedimentary environment more than seasonal cycles in primary production.

Eddy Correlation Benthic O_2 Exchange Rates and Characterization of Sediment Properties from the Central Oregon Shelf at 30 Meters

by
Kristina McCann-Grosvenor

A THESIS

submitted to

Oregon State University

in partial fulfillment of
the requirements for the
degree of

Master of Science

Presented December 10, 2010
Commencement June 2011

Master of Science thesis of Kristina McCann-Grosvenor presented on December 10, 2010.

APPROVED:

_____

Major Professor, representing Oceanography

_____

Dean of the College of Oceanic and Atmospheric Sciences

_____

Dean of the Graduate School

I understand that my thesis will become part of the permanent collection of Oregon State University libraries. My signature below authorizes release of my thesis to any reader upon request.

_____

Kristina McCann-Grosvenor, Author

ACKNOWLEDGEMENTS

Those who dwell, as scientists or laymen, among the beauties and mysteries of the earth, are never alone or weary of life.

~Rachel Carson

This project has been a large collaboration, and there are many people who have contributed in major and minor ways. I've been encouraged and supported by countless people throughout my time as a student, but first and foremost I would like to thank my advisor, Dr. Clare Reimers. This research would not have been possible without her guidance and amazing ability of foresight, not to mention the endless hours she spent patiently working with me, teaching me, and improving my understanding of the research, as well as the quality of my writing through her editor's discernment. In addition to Clare, I owe much appreciation to Peter Berg for the guidance he gave to Clare and I in the general application of this new method, along with generously sharing his data reduction programs; as well as to my lab mate Rhea Sanders for sharing her general knowledge of research, cruise prep, and sample analysis, along with going through all of the ups and downs of pregnancy and new motherhood with me during my time as a graduate student.

I would also like to thank my committee members and acknowledge the hard work of Tuba Özkan-Haller for all of her help with the physical oceanography questions that came up often and for being our MATLAB guru, and

to Fred Prahl and my grad rep Virginia Weiss for their input on my thesis and research.

The research assistants at COAS, as well as the marine techs also contributed a lot of help. Many thanks to Joe Jennings and Margaret Sparrow for all of their sample processing as well as always being happy to lend a hand on the cruises, and to Chris Romsos for making the maps of our lander deployments to include in this thesis as well as my talks. I also owe a big thank you to Dave O'Gorman for saving our new Control Unit as well as our computer while at sea through his brilliant soldering abilities and techie know-how, and also to Daryl Swensen and the crews of the R/V *Wecoma* and R/V *Elakha* for all of their assistance with our deployments. There are many other people who contributed to our cruises, but in particular I would also like to thank Cara Fritz, Maziet Cheseby, Yanming Gong, Cody Doolan, and Scott Barker for all of their help with coring and sediment sampling.

There are also numerous people who added to the quality of my time as a student, as well as to my experiences at Hatfield. I would like to give a particular thank you to all of the graduate students at the Hatfield Marine Science Center (past and present) for all of their advice and support throughout, as well as to my old lab mate Mark Nielsen, who was a wonderful mentor and dive buddy during that first year, I miss you Mark! I would also like to acknowledge the funding I received from the Mamie Markham Research Award through the Hatfield Marine Science Center.

Outside of the academic world I have had a tremendous amount of support and have been lucky to have such amazing and wonderful people in my life. Words cannot express the gratitude I feel towards my friends in Newport, Corvallis, Portland, and around the world, my community in Summit (who have become like family), and of course my family: my mom Lynn, my dad Dick, my grandpa Bob, my grandma Luella, my oldest and greatest friend Cindy (and her mom Connie and sisters Lori and Joy), my sister Trish, my nephew Geoff, my niece Kylie, my in-laws Gil and Wiley, Chris and Donna, Lexi and Dave, and Graham. Thank you all so much for believing in me.

At last, my deepest gratitude goes to my husband, Hovey and our daughter, Lilou, for always being supportive of me and for bringing such joy into my life. Hovey always helps me see the lighter side of things and I can't imagine exploring this wonderful world with anyone else.

TABLE OF CONTENTS

LIST OF FIGURES

LIST OF TABLES

Table Page

LIST OF APPENDICES FIGURES

Eddy Correlation Benthic O_2 Exchange Rates and Characterization of Sediment Properties from the Central Oregon Shelf at 30 Meters

Kristina McCann-Grosvenor

Master of Science Thesis

Presented December 10, 2010

INTRODUCTION

The Oregon Inner Continental Shelf underlies waters impacted by the California Current System. During the summer, north winds tend to dominate, bringing cold, high salinity water onto the shelf as a result of Ekman transport (Kirincich et al., 2005). The low oxygen (O_2) water introduces nutrients that replenish the existing depleted waters, producing phytoplankton blooms and increasing particulate organic matter (POM) concentrations (Hill and Wheeler, 2002). O_2 consumption increases as labile phytoplankton detritus is transported along the shelf, sinks and is respired (Wetz et al., 2008). Breaking waves and turbulence reoxygenate the shallow water column, and benthic decomposition is enhanced or sustained by the pumping action of waves through advective pore water flow (Jahnke et al., 2000; Huettel et al., 2003; Franke et al., 2006; Rusch et al., 2006). The increased respiration and benthic decomposition may contribute to shelf hypoxia (defined as low O_2 water, <63 μM O_2) (Grantham et al., 2004). Additionally, organic matter oxidation rates are flow-dependent in sandy sediments, and may be regulated more by physical than biological conditions (Reimers et al., 2004). This research investigates benthic O_2 flux and its temporal variation on the Oregon shelf, as well as how the Oregon shelf compares to other near-shore environments..

Sediment-water O_2 flux is an important measurement for understanding organic matter cycling, including utilization of O_2 and food supplied from waters above (Glud, 2008). Benthic-pelagic coupling is significant to our understanding

of near-shore environments and the benthic response to water column activity (Rowe et al., 1976). Currently limited O_2 flux data exists for the Oregon shelf (Severmann et al., 2010) due to the difficulty of implementing research or obtaining measurements in high-energy, sandy environments. Regionally, as well as globally, the rates of benthic biogeochemical processes and impacts on near-shore environments are not well known (Rowe et al., 1988; Grantham et al., 2004). Understanding current relationships is important since the coastal ecosystem may be altered in the near future due to installation of wave energy technologies (Boehlert and Gill, 2010), changes in fishing pressure (Pinnegar et al., 2000; Tegner and Dayton, 2000; Pauly et al., 2002), increased hypoxic events (Hill and Wheeler, 2002)(Grantham et al., 2004) (Bograd et al., 2008)(Chan et al., 2008)(Connolly et al., 2010), and climate change (Jackson et al., 2001; Harley et al., 2006; Keeling et al., 2010). Time series measurements are necessary for examining temporal variations and predicting climatic changes, as well as setting a baseline prior to installation of wave energy buoys.

Measurement of in situ O_2 exchange rates with permeable sediments, such as those found over ~43% of the Oregon-Washington shelf (Romsos et al., 2007), has traditionally been difficult. The most widely practiced technique, a benthic chamber, measures O_2 consumption in a relatively small, enclosed area of seafloor (commonly 0.02 m^2 – 0.1 m^2) (Reimers and Smith, 1986; Archer and Devol, 1992; Tengberg et al., 1995; Janssen, Faerber, et al., 2005; Glud et al., 2009) that usually encompasses ≤10L bottom water, thereby eliminating some O_2

transport processes such as advection driven by pressure gradients (Huettel and Webster, 2001; Berg et al., 2003, 2009; Kuwae et al., 2006; Berg and Huettel, 2008). Exclusion of such processes can cause an underestimation of O_2 flux in environments impacted by waves (Berg and Huettel, 2008). In addition, it is also difficult to obtain a seal around the bottom of chambers when sampling in sandy sediments. Core incubations, an alternative means to measure O_2 exchange rates, are conducted in a controlled laboratory environment and do not quantify in situ O_2 flux due to the difficulty in maintaining in situ conditions (light, water temperature, pressure and flow). Measurement of O_2 consumption in the enclosed, overlying water eliminates transport processes, similar to chambers, but may also limit irrigation by macrofauna. Both methods are also limited in their implementation, and cannot accommodate hard bottom or rocky substrates (Berg et al., 2003; Kuwae et al., 2006). Microprofiling, another method traditionally used that is based on in situ measurements of O_2 profiles across the sediment-water interface, derives vertical diffusive fluxes only. Thus, microprofiling does not capture O_2 exchange due to bioirrigation and current or wave-induced advection. In addition, microprofiles sample only a very small area (~0.01 cm^2) of seafloor with each profile (Berg et al., 1998, 2003).

In contrast, the Eddy Correlation (EC) method is a non-invasive technique adapted from atmospheric boundary layer research and developed for the benthic boundary layer by Berg et al. (2003, 2007, 2009) that allows measurements of total benthic O_2 exchange at high temporal resolution under

true in situ conditions with minimal, if any, disturbance of the sediment or hydrodynamic flow (Berg et al., 2007). The EC method reflects exchange processes occurring in an area of seafloor up-current of the instrument site, and assumes (1) that there is no storage or loss of O_2 within the benthic boundary layer; (2) the seafloor is a homogenous, horizontal local source or sink for O_2; (3) all oxygen exchange (OE) is the result of turbulent eddies; (4) all eddies contributing to the turbulent fluctuations are captured during the sampling period; and (5) above the diffusive boundary layer turbulent advection is the dominant transport process, therefore diffusive contributions and horizontal advection can be neglected (Berg et al., 2003, 2007).

Using EC, O_2 flux is determined from simultaneous measurements of the fluctuating vertical velocity and fluctuating O_2 concentration in $\sim$1 cm^3 of water, and these measurements are sensitive to benthic processes over a large area of seafloor (depending upon the measurement height above the surface and the sediment surface roughness) (Berg et al., 2007). In this work we use the EC method to evaluate benthic O_2 exchange rates in a dynamic inner-shelf environment off the central Oregon coast. The data collected allow us to assess benthic O_2 fluxes throughout the upwelling season, contributing to our understanding of O_2 utilization by the benthos under the effects of variable waves and currents, as well as during episodes of increased organic matter input. In addition, we use in situ microprofiles to assess pore-water O_2 concentration and O_2 penetration depths, and sediment cores to characterize the chemical and

physical properties of the seabed within the study area.

MATERIALS AND METHODS

Study Site

The study was conducted in the eastern North Pacific Ocean at approximately 44.7°N 124.1°W, a site adjacent to the Newport Hydrographic line off the Oregon Coast, where the mean water depth is ~30m (Figure 1) (Appendix B, Table B-1). EC measurements, water column sampling, and sediment sampling were conducted between late March and late October 2009 aboard OSU research vessels. March, June, August, and October cruises were 4-8 days in length on *R/V Wecoma*, whereas April, July, and September cruises utilized the *R/V Elakha* for 1-2 days.

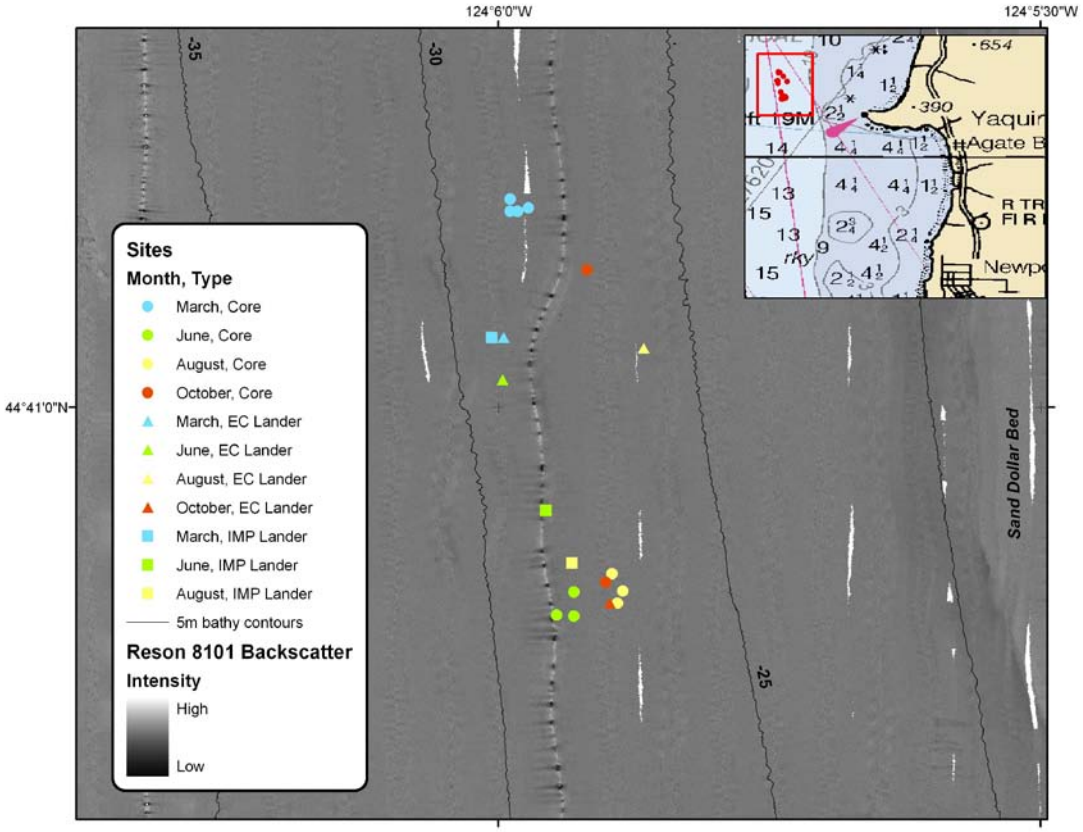

Figure 1 Map indicating locations for the EC and IMP lander deployments and core samples (see legend). Backscatter shows uniform seabed, bathymetric lines indicate depth regions. Inset map shows location in relation to Yaquina Head, Newport, Oregon.

Eddy Correlation Methodology

Theoretical descriptions of the effects of turbulence on a scalar quantity such as dissolved O_2 (C) classically begin by separating C and velocity components parallel to x, y, and z into mean and fluctuating quantities (e.g., $\overline{C}$ and C'; $\overline{u_i}$ and u_i'). Under the eddy correlation (EC) method it is assumed that stationary and homogeneity conditions are fulfilled (Aubinet, 2008) so that the covariance between fluctuating vertical velocity (u_z') and O_2 concentration (C') allows derivation of the vertical O_2 flux (Berg et al., 2009, 2003):

$$\overline{Flux} = \overline{u_z' C'}$$

where the 'bar' represents averaging over a time period (5-15 minutes for our data sets). As well, EC fluxes can be calculated in the frequency domain:

$$\overline{Flux} = \int_0^\infty Co_{u_z' C'}(f)\,df$$

where $Co_{u_z' C'}$ is the cospectrum of the turbulent fluctuating vertical velocity and dissolved O_2 concentration and f is the frequency. Both formulations are used in this study to evaluate benthic eddy fluxes of dissolved O_2.

Instrumentation

Eddy Correlation Systems

Two different systems were used to measure the parameters needed to derive benthic EC O_2 fluxes on the shelf of the Oregon coast. The main system utilized, the 'Berg System' (ECB) (Figure 2), assembled by Unisense A/S (Aarhus Denmark), is similar to the original instrumentation used by Peter Berg for his initial eddy correlation (EC) research (Berg et al., 2003). This instrumentation includes a fast responding microelectrode O_2 sensor mounted in an oil-filled pressure-compensated holder (to prevent implosion of electrode) connected to an auto-zeroing amplifier (developed at the Max-Planck Institute for Marine Microbiology, Bremen Germany) that is cabled to a Vector Acoustic Doppler Current Meter (Nortek AS, Norway). The Vector is battery powered and serves as the system data logger. During the study period a newly developed eddy correlation 'Unisense System' (ECU) (Figure 3) was also employed. It was designed by Unisense A/S and is similar to the ECB system with the added benefits of a separate control and data logging unit and the option to add supplementary sensors. The control unit provides a rechargeable battery pack, and its own unique software for sensor calibrations and data recovery.

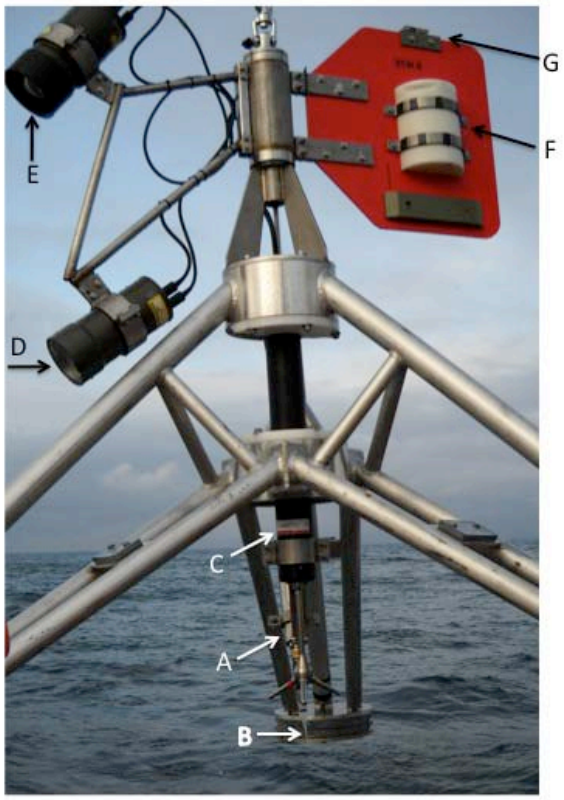

Figure 2 EC 'Berg' System includes a Max Planck AZ amplifier (A) that is attached to an O_2 microelectrode (B), and a Nortek Vector ADV (C) that acts as the data logger. A digital camera (D) and strobe (E) (Scorpio) are located on a rotating bearing assembly with vane that holds the battery pack (F), as well as the Wildlife Computer MK9 light, temperature, and pressure sensor (G) which was added in June.

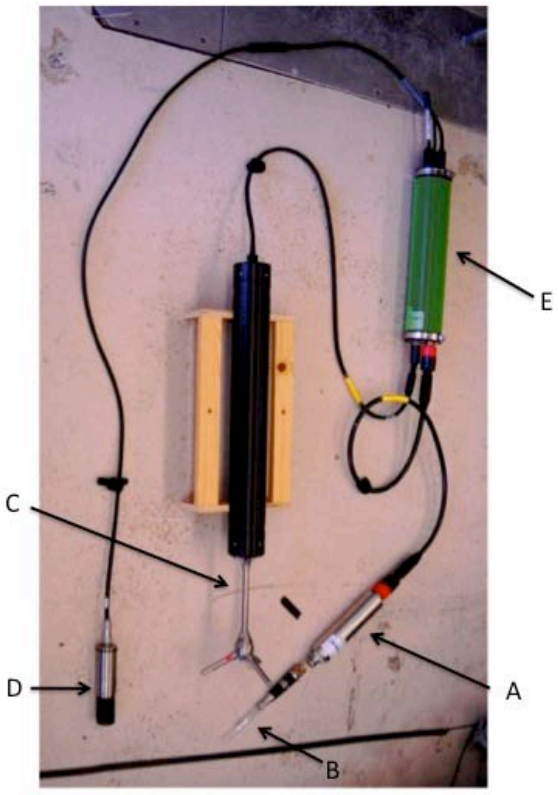

Figure 3 EC 'Unisense' system includes a Max Planck AZ amplifier (A) that is attached to an O_2 microelectrode (B), a Nortek Vector ADV (C), Aanderaa O_2 optode (D), and a control unit (E) that acts as the data logger.

O_2 Sensors

O_2 concentration measurements for the EC calculations were made using microeletrode O_2 sensors built in C. Reimers' Lab at the Hatfield Marine Science Center (Newport, OR) or by Unisense A/S (Denmark) following the Clark-type sensor model (Revsbech, 1989). Tip outer diameters ranged from 4-25 μm with a signal of 3-17 pA in anoxic solution (Appendix A, Table A-1). A preliminary assessment of each sensor was made using a picoammeter (Unisense PA2000) and data recorder (Agilent 34970A) connected to a lab computer. The O_2 sensors were polarized until the signal was steady (3-82 hours), then a two-point calibration was performed (assuming the sensor response to O_2 concentration is linear). A 10% solution of 1M Na-ascorbate and 0.5 M NaOH was used to acquire a zero reading for the sensors (Andersen et al., 2001) and air-saturated seawater was used to obtain a second calibration point. Repeat calibrations for the sensors were also made at sea before and after deployments. Final calibrations applied to the EC time series were based on preceding Na-ascorbate zero readings and a second point derived by matching an in situ sensor reading averaged over one burst to a corresponding O_2 concentration determined simultaneously from a bottom water Winkler titration. An Aanderaa (4175) O_2 optode was added to the ECU system and mounted on one of the tripod legs to obtain independent, ambient O_2 measurements (August only).

Amplifier

The Max Planck AZ amplifier connects to a pressure compensated O_2 microelectrode holder and separates the O_2 microelectrode signal into two components: AC, the oscillating O_2 signal; and DC, the average O_2 signal. The All signal is the combination of AC + DC. The AC signal is amplified 10x compared to the ALL signal. Thus, we utilized the AC signal for our O_2 flux calculations.

Vector

The Vector (6MHz VEC 3285) is a 3D acoustic Doppler current meter (Nortek AS) that measures water velocities in x, y, and z coordinates at high rates using bistatic sonar. It also measures pressure, temperature, tilt, and compass heading, and contains an internal battery and memory. The titanium probe is composed of a transmit transducer in the center and three arms with receive transducers positioned off to the side. The transmit and receive beams intersect at a sampling volume, 157mm below the transducer. The O_2 microelectrode tip is positioned adjacent to this sampling volume (8-20 cm above the sediment surface, see Appendix A, Table A-2) and simultaneously measures O_2 concentrations (Figure 4). In order to reduce noise in the data, Nortek allows different range settings for the Vector depending upon site conditions. Our Vector's range was set at ±0.3 m/s (the lowest possible velocity setting that would not exceed horizontal or vertical velocity at our study site) and sampling rate was set at 64Hz, for 15-minute bursts with 5-minute rest periods between bursts.

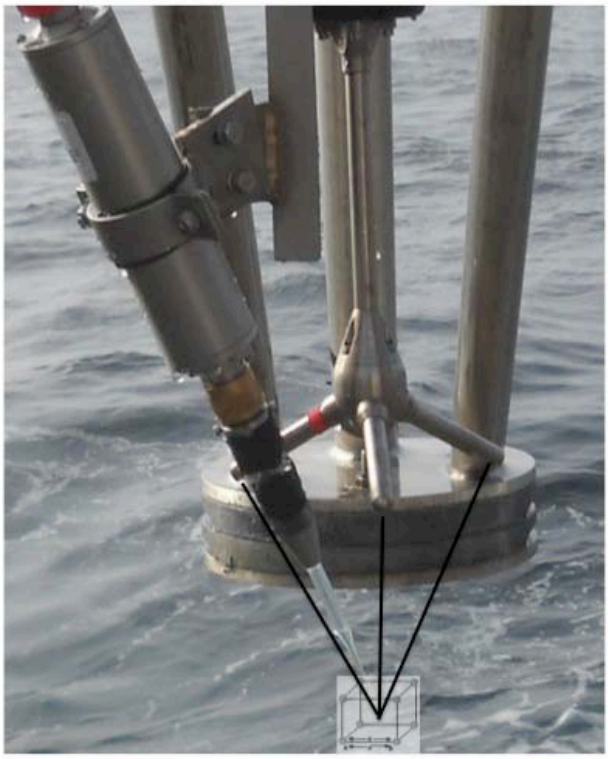

Figure 4 The O_2 microelectrode and Nortek Vector sample the same volume of water at some distance above the sediment floor (8-20cm)

CTD

A Conductivity-Temperature-Density sensor (Seabird SBE 37SM) was attached to a leg of the EC lander and set to take measurements every five minutes during *R/V Elakha* cruises. On *R/V Wecoma* cruises, the ship's CTD-rosette system (Seabird SBE 911 Plus) was utilized to measure full water column profiles.

Landers

Eddy Correlation Lander

An aluminum tripod, 1.8m x 2.3m, with lead-weighted feet (~450lbs) was designed and constructed at OSU for benthic EC flux data collection (Reimers et al., 2010). The EC instruments were mounted at the center of the lander. A digital time-lapse camera and strobe light (Insite Pacific Inc. Scorpio Plus underwater digital still camera) were mounted at the tripod's apex on a rotating ball bearing assembly with a fin to guide the camera into the current (Figure 2). The camera provided images of the seafloor area surrounding the lander. In June an Mk9 light meter (Wildlife Computers) was mounted on top of the camera counter-balancing vane to measure light intensity at the site (using a logarithmic response), and included additional temperature and pressure sensors.

In Situ Microprofiler (IMP)

The IMP was deployed to measure pore-water O_2 and formation factor profiles at the study site during each *R/V Wecoma* cruise. The lander was equipped with 2-4 Clark-type O_2 microelectrodes (Revsbech, 1989) connected to external preamplifiers within pressure-compensated holders, along with a four-wire

resistivity sensor (Reimers et al., 1992). These sensors were mounted in a circular array on a motorized profiler that was programmed to lower the sensors in vertical steps of 0.125mm, recording fine-scale O_2 concentration and resistivity measurements across the sediment-water interface and into the sediment. Calibrations of the O_2 microelectrodes were made against laboratory measurements, bottom-water O_2 concentrations through Winkler titrations, and anoxic pore-water measurements (Reimers and Glud, 2000). The microelectrode data were converted to O_2 profiles, and resistivity vertical profiles were converted to formation factor values as in Reimers et al. (1992).

Hydraulically-Dampened Gravity Corer (HDGC)

Sediment cores were recovered with a HDGC designed to sample sandy sediment without pore water loss and with little disturbance to the sediment-water interface. Each acrylic core tube had an approximate length of 94 cm with an inner diameter (ID) of 11.43 cm. The HDGC was deployed during each *R/V Wecoma* cruise and sediment cores (~30–57 cm) were transferred immediately to a refrigerated van (T = 8±2° C) where they were later subsampled.

Eddy Correlation Data Reductions and O_2 Flux Calculations

Recorded Vector and microelectrode data were converted into time-series -ascii files through the Vector program software (ECB system) or Unisense program software (ECU system). The ECB system files were processed through ExtractNortekVer1.3 software (Berg, 2008) to extract the amplifier data and convert it into O_2 concentration (μM) according to our O_2 microelectrode calibrations. Outliers were removed from raw O_2 and raw velocity data by MATLAB programs, using a phase-space method (Goring and Nikora, 2002) modified by Tuba Özkan-Haller for this study, replacing all outliers with a 3rd order polynomial spline. Clean data was reduced from 64Hz to 16Hz using ReduceHzVer1.1 software (Berg, 2008) to condense high-frequency noise.

Two mean removal methods were compared, 'flux 2' (linear detrending) and 'flux 3' (running mean detrending) (Berg et al., 2003). We determined that the practice of rotating the coordinates every burst to meet the condition of $\overline{u_z} = 0$ (Berg et al., 2003) distorted the flux calculations by removing low frequency contributions; therefore this approach was not favored. Instead we did not rotate the coordinates and it was assumed the sum ensemble of $\overline{u_z} * \overline{C} = 0$ (but for comparison, rotation results are reported in Table 2).

Furthermore, for the ‘flux 3’ mean removal method using a running average, we routinely chose N_r=3601 data points (see Figure 5). This should have the effect of filtering out from u_z and C the low frequency trends that could be caused by undesired factors such as horizontal advection or electrode drift.

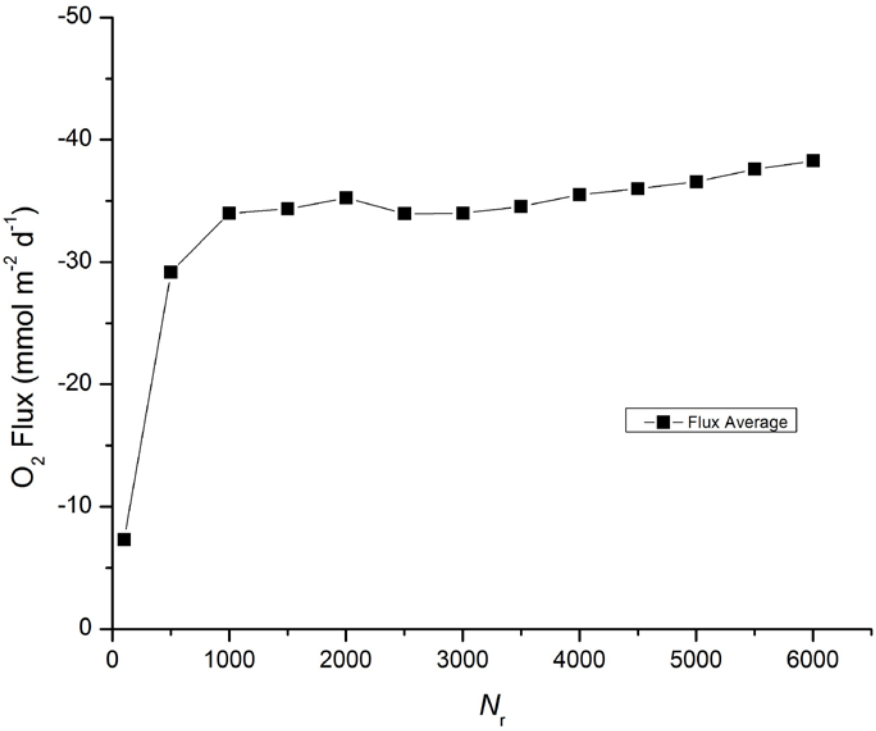

Figure 5 Illustration of average O_2 flux dependence on the number of data points (N_r) included in the running mean for flux 3 calculations. O_2 flux attains a near-constant value by N_r=3601. Data are from June deployment.

O_2 flux was calculated in the time domain using EddyFluxVer1.8 software (Berg, 2008). In order to avoid errors in flux calculations caused by a breakdown of the method assumptions, portions of bursts were excluded if there were large progressive increases or decreases of bottom water O_2 concentration, or sections of rapidly changing current direction in the velocity data; this left bursts of varying length between 5-15 minutes. Flux calculations were also run repeatedly for each screened burst removing the means using an increasing running average N_r=101, 1001, 2001, 3001, and 4001. The results were graphed per burst in order to eliminate any burst in which the flux did not obtain a near-constant value by N_r=3601 (see Figure 6). Total and cumulative flux values were accepted for those bursts that flux 2 and flux 3 cumulative calculations had similar linear progressions and values, as well as the total flux value reaching a near-constant value by N_r=3601.

The flux contribution was also analyzed in the frequency domain using a Matlab co-spectrum program (Ozkan-Haller, 2008) allowing us to quantify frequencies that contribute to the vertical O_2 flux. In addition, this program uses the Vector pressure data to calculate wave period and significant wave height from the vertical accelerations of waves detected at the bottom.

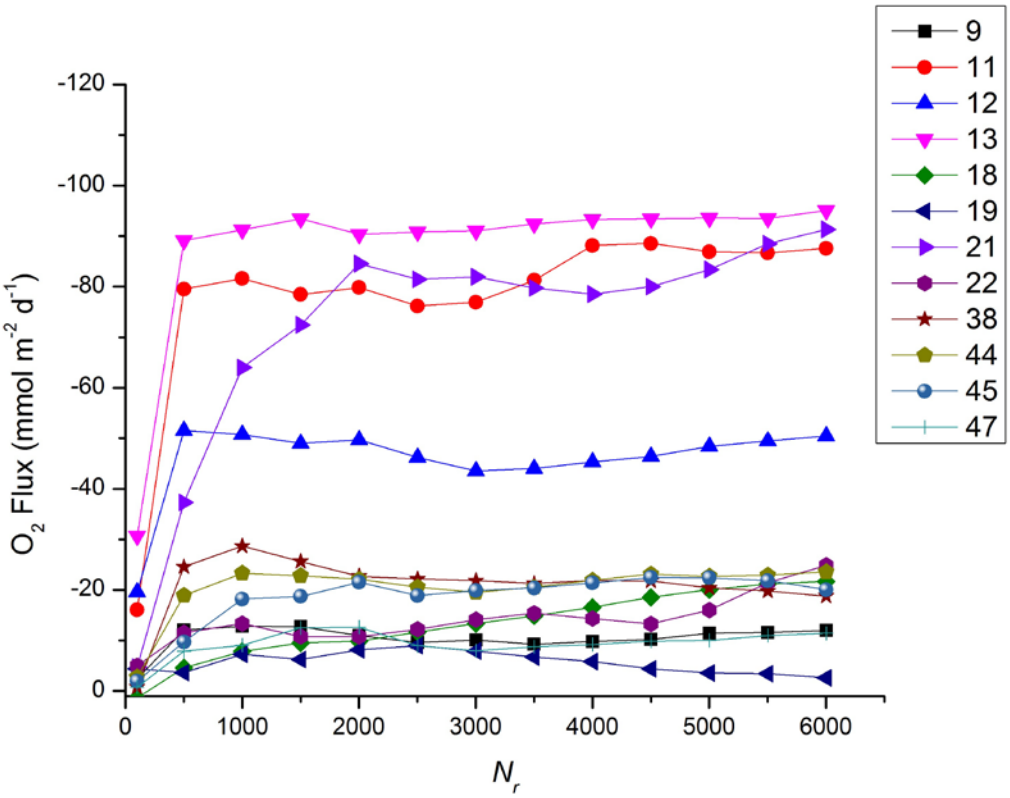

Figure 6 Illustration of dependence of O_2 flux concentration on the number of data points (N_r) included in the running mean calculation for individual bursts (average for all bursts is shown in Figure 5). Legend depicts "Burst #" during deployment. Burst #1 would correspond with the start of a deployment (time 0-15 minutes), Burst #9 corresponds with time 160-175 minutes (see Table 2 for actual edited times included in flux calculations). This method was used to identify bursts that did not reach a near-constant value by N_r=3601 (ie-bursts 1-8, 10, 11, 14-17, 20, 23-37, 39-43, 46, and 48 were excluded from the final calculations for June).

Sediment Samples

All cores taken with the HDGC were inspected and those with no or minimal disturbance were kept for subsampling. A compressed air-powered core extruder, designed and built at Oregon State University (OSU), was used in the cold van to extrude long cores into 1-cm intervals (from 0-5 cm) and 2-cm intervals (from 5-52 cm) that were then subsampled for further analyses. The top ~20 cm of select long cores were extruded into permeability core tubes for permeability measurements in the lab (Rocha et al., 2005).

Grain Size

A laser diffraction particle size analyzer (PSA) (Coulter LS100Q) was used to determine particle size distributions of a subset of samples following the Environmental Protection Agency's (EPA) procedure of digestion using H_2O_2 to remove organic matter, revised from Ingram (1971). Prior to introduction into the PSA sample chamber, aliquots of sediment samples were well mixed in water by a high speed, reversing mixer. The PSA performed four determinations for each sediment aliquot.

Weight Percent Fines

An estimate of the weight percent of fines (or weight percent of silt and clay) in down-core samples was determined based on Stokes' Law of particle-settling velocity, which states that terminal velocity of a free-falling sphere in seawater is related to its diameter (larger particles settle faster than small ones). Sand is

classified as any particle with a diameter between 62 μm - 1 mm, silt is between 2-62 μm, and clay is everything with a diameter less than 2 μm (Burdige, 2006). A subsample (2 cm^3) from each sediment layer was placed in a 15 cm^3 BD Falcon conical centrifuge tube and covered with 3 cm of filtered seawater from bottom water POC collections. The sample was shaken vigorously, after which it was allowed to stand undisturbed for 10 seconds. The suspension was pipetted off and suspended particles were collected on a pre-weighed filter (25 mm Whatman GF/C). All quartz-density particles ≤62 μm should remain suspended using this method. This process was repeated until the water appeared clear, usually five times per sample. The filter was then rinsed with deionized water, wrapped securely in foil and stored in -80C freezer. At a later date filters were dried and reweighed.

Permeability and Porosity

Permeability was measured after transferring the uppermost 18-21 cm of selected HDGC cores to acrylic core tubes (30-cm long, 9.5-cm ID). They were then plugged with plastic bottoms fitted with o-rings for a watertight seal and a filter to prevent loss of sediment through the drainage hole, then stored in a cold van (T=8±2° C) on ship for the duration of the cruise. Once on land, permeability cores were transferred into a cold room (T=10±2° C) and measurements were conducted using a falling head permeameter (Rocha et al., 2005) that measures the flow rate through the core by monitoring pressure with an in-line pressure

transducer. The analog output of the pressure transducer was recorded every 10 s in mV. Permeability is calculated from hydraulic conductivity:

$$\kappa = \left(\frac{aL}{At}\right)\ln\left(\frac{H_0}{H_f}\right)$$

where a is the cross-sectional area of stand pipe (cm^2), A the cross-sectional area of the sediment core (cm^2), L the length of the sediment core (cm), t the time elapsed during data collection (s), H_0 the head of water in the stand pipe at t=0 (mV), and H_f the head of water in the stand pipe at final t (mV).

Porosity (ϕ) was measured down-core from HDGC core subsamples, calculated with a particle density of 2.54 g cm^{-3}, and determined from weight and water displacement:

$$\phi = 1 - \frac{sample\ dry\ mass}{sample\ total\ wet\ volume \times \rho_{particle}}$$

Sediment dry mass was measured after being rinsed with deionized water and dried at 60˚ C.

Sediment Chlorophyll

Sediment samples (2 cm^3) were extracted with 90% acetone for 24 hours at 4° C in the dark. Extracted samples were centrifuged five minutes to consolidate particulates. Supernatant was poured off into a syringe (30 mL Luer Lock) with filter (0.45 µm GFC Luer Lock) attached. Chlorophyll and phaeopigment concentrations were determined fluorometrically (Turner Designs AU10) (Strickland and Parsons, 1972). Duplicates were run randomly approximately

every sixth sample. The rpd values were calculated as the absolute value of the difference between each set of duplicates divided by their average, then multiplied by 100. Chlorophyll concentrations were low in general causing any elevated value to skew averages computed for grouped depth intervals, resulting in seemingly high variability among duplicates (see results).

Sediment TOC/TN

Approximately ¼ of each depth interval was separated and stored in LDPE, snap closure 4 ¼ dr Nalgene vials. These samples were ground, and splits were placed in silver boats followed by tin boats (9x15 mm) then acidified by concentrated HCL fumigation to remove carbonates, modified from Verardo (1990). TOC/TN was measured by automated combustion (Carlo Erba NA1500 Series 2 elemental analyzer) with acetanilide as the calibration standard.

Water Samples

Bottom water samples (1-5 m above the seafloor) were taken using Niskin bottles on a CTD-rosette system during each EC deployment on *R/V Wecoma*. Onboard, aliquots were promptly drawn for O_2, nutrient, salinity, Particulate Organic Carbon (POC) and Nitrogen (PN), and chlorophyll analysis. During *R/V Elakha* cruises, bottom water samples were taken with individual wire-clamped Niskin bottles for O_2 samples only.

Dissolved O_2 concentrations were determined by Winkler titration as in Culberson (1991). Information on additional bottom water analyses from *Wecoma* cruises is available from C. Reimers (OSU).

RESULTS

Eddy Correlation Measurements

Six successful eddy correlation deployments were carried out at the study site during six separate months, resulting in four to fifty-eight 15-minute bursts of data per deployment. Other unsuccessful deployments were made each in March, April and October (data not shown due to the O_2 sensor being faulty or broken during deployment or sampling height being in a weak spot for the Vector, which corrupts the data). Of the successful deployments, bottom water O_2 concentration was lowest in August (ranging from 101 to 159μM) and highest in October (ranging from 221 to 299μM) along with bottom water temperature (as measured by the Vector) being the lowest in July (ranging from 8 to 9˚C and showing evidence of upwelling) and highest in October (ranging from 11 to 13˚C)[1]. Mean current speed for individual bursts was weakest in September (ranging from 0.4 to 6.2 cm s^{-1}) and strongest in August (ranging from 4.2 to 6.7 cm s^{-1}), which corresponds to the months with a large change in current direction (September) and essentially no change in current direction (August) as is discussed later. Bottom detectable significant wave height[2] was the smallest in July (ranging from 0.4 to 0.6 m) and largest in March (ranging from 1.7 to 2.1 m), while wave period was also the shortest in July (ranging from 6.5 to 7.6 s) but

[1] Note: the Vector temperature sensor has a slow response so the temperature signal often shows hysteresis at the start of deployments (e.g., Figure 8). The temperature records were not despiked of noise in the plots presented.

[2] Significant wave height is usually defined as the average 1/3 of surface waves measured over an interval of time. Because records of wave height in this study were derived from changes in bottom pressure, small waves would have not been detected, causing our estimates of H_{sig} to be slightly biased towards larger waves.

longest in June (ranging from 7.4 to 18.4 s) (Table 1). Velocity, pressure, O_2 concentration, and temperature data are shown for all months (Figures 7, 8, 9, 10 and see Appendix A, Figures A-2 and A-4). In August, the ECU system was utilized, and Figure 9 shows the optode data plotted with the microelectrode data. Their similar trends confirm the temporal variability of O_2 using two separate methods for data collection. June, July and September time-series also show temporal changes. Corresponding changes in the velocity, pressure (falling and rising tide), temperature and O_2 data can be seen between t=240 and 800 minutes during the June deployment (Figure 7). In the beginning of the July deployment abrupt changes in the velocity occur, and pressure change (falling and rising tide) as well as slowly decreasing O_2 concentration are visible during the deployment (Figure 8). During the September deployment, abrupt changes in the velocity occur throughout but are most notable between t=660 and 960 minutes, which corresponds with changes in O_2 and temperature as well as the tidal change in pressure (Figure 10).

Table 1 Burst averages of bottom-detectable significant wave height and wave period (calculated from the Vector pressure data), mean vertical velocity (calculated from Vector velocity data in the z-direction), and current speed (calculated as the absolute value of the resultant of the mean velocities in the x, y and z-directions), n=number of bursts.

Month	H_{sig} (m)	SE	T_p (s)	SE	V_z mean (cm s^{-1})	SE	V mean (cm s^{-1})	SE	n
March	1.86	0.14	10.32	0.31	-0.61	0.10	5.24	0.50	4
June	0.65	0.06	16.11	2.56	-0.36	0.27	4.46	2.37	57
July	0.44	0.06	7.02	0.28	-0.24	0.14	2.83	1.26	36
August	1.48	0.12	8.77	0.80	-0.62	0.10	5.50	0.65	17
September	1.06	0.11	10.52	0.85	-0.23	0.11	2.36	1.35	57
October	1.67	0.15	8.64	0.46	-0.01	0.00	4.18	1.13	15

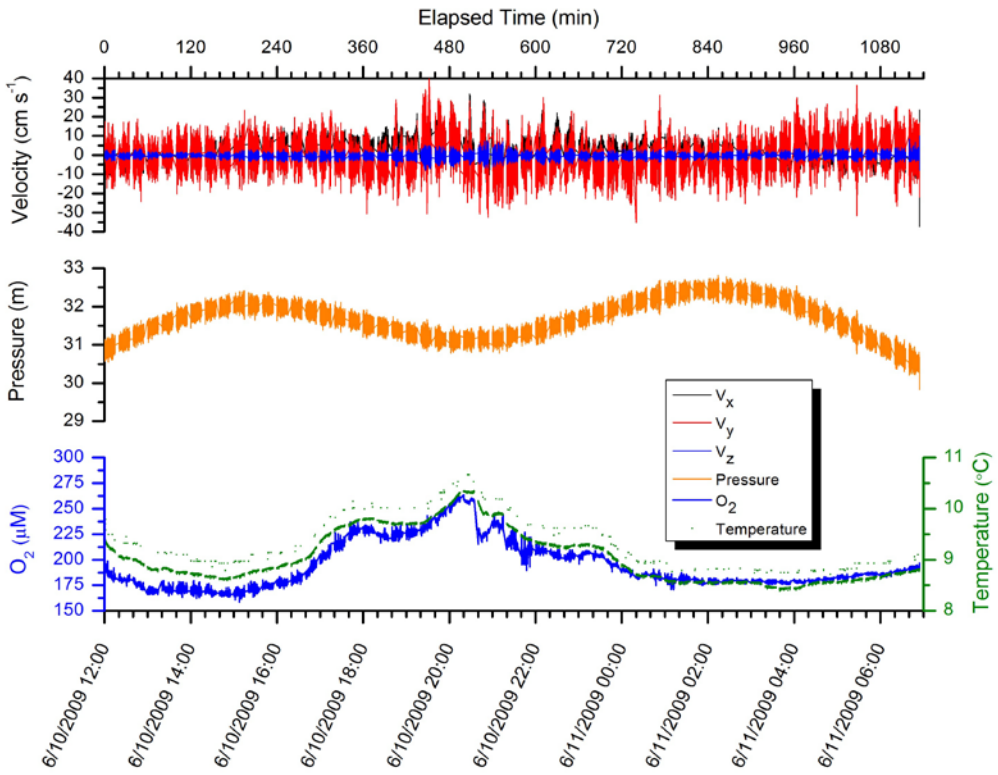

Figure 7 Despiked 16-Hz velocity data (x, y, z) (top), pressure data (middle), and O_2 microelectrode and temperature data (bottom) for total deployment time in June. Upper x-axis depicts time elapsed from instrument start time; lower x-axis depicts date and time.

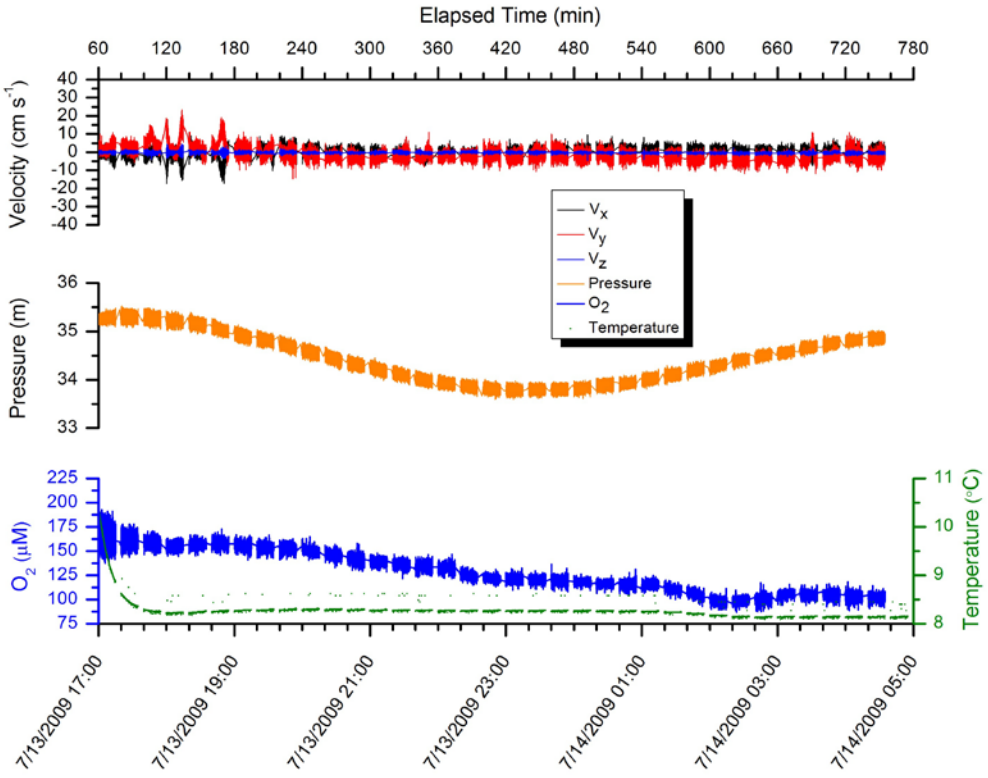

Figure 8 Despiked 16-Hz velocity data (x, y, z) (top), pressure data (middle), and O_2 microelectrode and temperature data (bottom) for total deployment time in July. Upper and lower x-axis same as Figure 7.

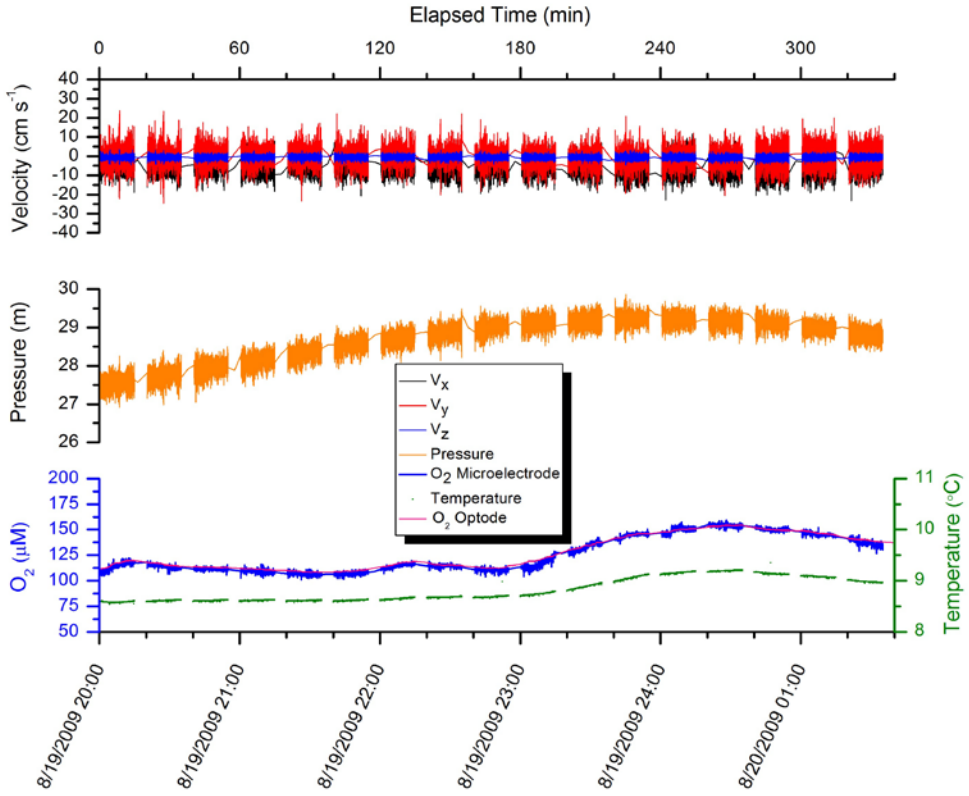

Figure 9 Despiked 16-Hz velocity data (x, y, z) (top), pressure data (middle), and O_2 microelectrode and optode data along with temperature data (bottom) for total deployment time in August. Upper and lower x-axis same as Figure 7.

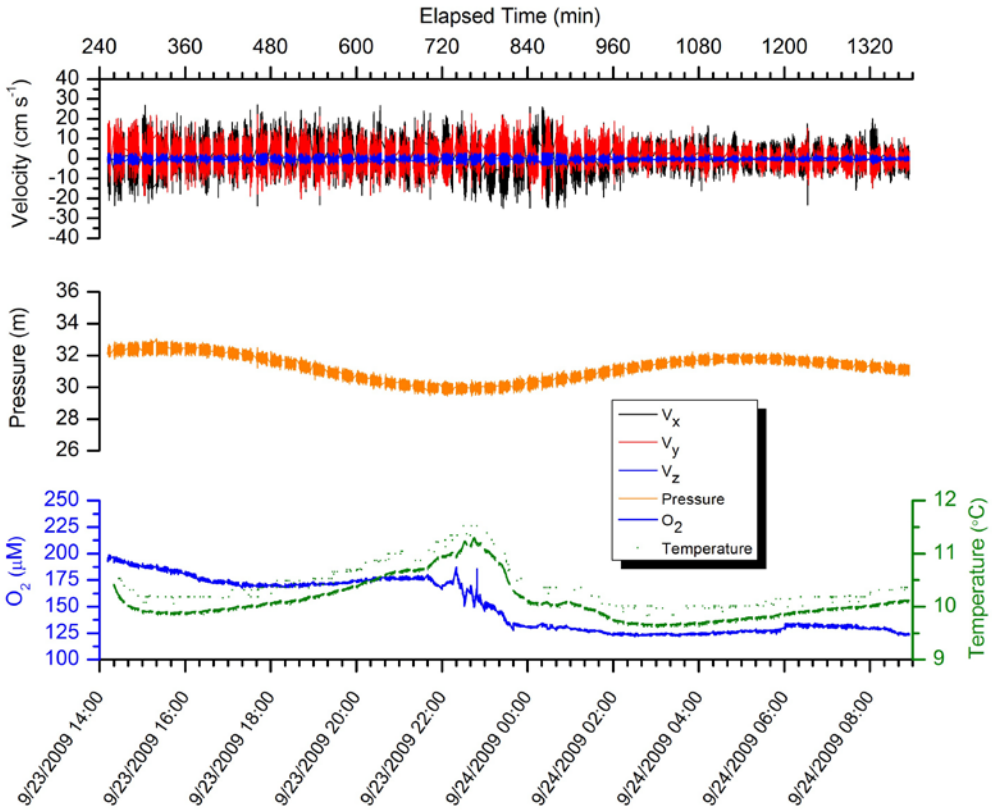

Figure 10 Despiked 16-Hz velocity data (x, y, z) (top), pressure data (middle), and O_2 microelectrode and temperature data (bottom) for total deployment time in September. Upper and lower x-axis same as Figure 7.

EC flux results for individual bursts are given in Table 2. Average O2 exchange ranged from 9.8 to 26.4 (flux 2) and 10.7 to 26.8 (flux 3) mmol m-2 d-1 (positive flux represents production by sediments) in March to -90.9 to -2.9(flux 2) and -92.0 to -6.9 (flux 3) mmol m-2 d-1 in June (negative flux represents consumption by sediments, also referred to as O2 uptake). Data collection time ranged from 1 hour 35 minutes (March) to 23 hours 29 minutes (July). Mean O2 exchange for each month was calculated from bursts that met criteria as explained in Methods. The number of acceptable bursts within each month has been reduced to 4 (March), 12 (June), 20 (July), 5 (August), 14 (September) and 15 (October) with record lengths between 5 and 15 minutes, depending upon the amount of data eliminated due to jumps in the O2 microelectrode or other issues (see Methods). Total time included in the flux calculations is 59.5, 98.5, 287, 60, 123, and 124.2 minutes (March, June, July, August, September, and October, respectively). Maximum O2 uptake rates in June took place between 3-7pm. Overall, O2 flux 2 varied from -2.9 to -90.9 mmol m-2 d-1 and O2 flux 3 varied from -6.9 to -92.0 mmol m-2 d-1 (bursts at t=360 and 241 min, respectively) (Figure 11). It is interesting to note that the temporal shifts in O2 concentration during the deployment (Figure 7) did not invalidate all the EC flux calculations, as the accepted bursts show strong linear cumulative fluxes that correlate well between the flux 2 and flux 3 methods (Figure 11).

Table 2 Eddy correlation flux 2 (linear detrending) and flux 3 (running average) mean removal calculation results per burst with time-weighted mean per month, unrotated and rotated. Total time per month is given in parenthesis.

Month	Time (min)	Unrotated Flux 2 (mmol m^{-2} d^{-1})	Unrotated Flux 3 (mmol m^{-2} d^{-1})	Difference	Rotated Flux 2 (mmol m^{-2} d^{-1})	Rotated Flux 3 (mmol m^{-2} d^{-1})	Difference
March	20.5-35	22.2	22.1	0.1	-136.3	-137.3	1.0
	40-55	17.4	25.7	8.3	-107.1	-100.2	6.9
	60-75	26.4	26.8	0.4	-53.1	-53.4	0.3
	80-95	9.8	10.7	0.9	-47.0	-46.0	1.0
Mean	(59.5)*	18.9	21.3	2.4	-85.5	-83.8	1.7
June	160.5-172	-10.9	-9.2	1.7	-16.2	-13.6	2.6
	209-215	-85.4	-81.2	4.2	-55.2	-53.0	2.2
	225-235	-60.9	-44.1	16.8	-38.4	-24.5	13.9
	242-255	-90.9	-92.0	1.1	-73.1	-75.5	2.4
	349-355	-20.0	-14.8	5.2	-45.9	-41.7	4.2
	368.5-375	-2.9	-6.9	4.0	-88.5	-93.5	5.0
	407-412	-77.6	-79.0	1.4	-144.2	-109.5	34.7
	429.5-435	-8.6	-15.4	6.8	-7.5	-7.4	0.1
	746-753	-26.6	-22.0	4.6	-0.8	2.8	3.6
	862-875	-19.3	-20.9	1.6	59.6	56.3	3.3
	881-891	-19.8	-20.4	0.6	-42.1	-34.1	8.0
	930-935	-11.7	-8.7	3.0	-11.8	-9.4	2.4
Mean	(98.5)*	-37.5	-35.7	4.3	-32.2	-28.3	6.7

July	180-195	-21.6	-8.1	13.5	-6.9	-4.7	2.2
	241-255	-10.4	-16.4	6	-16.2	-14.8	1.4
	280-295	-12.5	-11.7	0.8	-6.3	-3.3	3
	300-315	-33.2	-23.1	10.1	-37.0	-23.2	13.8
	320-332	-9.2	-9.3	0.1	-9.3	-9.4	0.1
	363-375	-12.8	-19.7	6.9	-11.9	-18.3	6.4
	400-415	-15.8	-12.3	3.5	-8.6	-9.6	1
	420-435	-17.0	-13.9	3.1	-13.4	-11.1	2.3
	440-450	-7.0	-6.1	0.9	1.8	3.1	1.3
	461-475	-7.0	-4.5	2.5	8.9	-2.9	11.8
	480-495	-16.4	-14.0	2.4	-6.4	-5.7	0.7
	500-515	-31.8	-17.4	14.4	8.4	-1.5	9.9
	520-535	-14.0	-11.6	2.4	-5.5	-3.7	1.8
	560-575	-7.6	-3.8	3.8	10.6	7.8	2.8
	580-595	-15.2	-11.2	4	1.3	2.0	0.7
	600-615	-9.9	-11.1	1.2	3.2	0.4	2.8
	660-675	-15.1	-31.6	16.5	7.7	-17.2	24.9
	700-715	-21.7	-14.2	7.5	-15.7	-8.0	7.7
	720-735	-13.1	-13.8	0.7	14.2	2.5	11.7
	740-755	-8.1	-9.2	1.1	-2.6	-2.9	0.3
Mean	(287)*	-15.2	-13.3	5.1	-4.2	-6.0	5.3
August	47-54	-18.6	-3.2	15.4	-7.6	8.7	16.3
	60-68	-7.6	-8.7	1.1	1.1	1.9	0.8
	80-95	-3.2	-7.1	3.9	2.5	-0.1	2.6
	120-135	-11.4	-10.5	0.9	2.1	-7.7	9.8
	260-275	-13.8	-1.7	12.1	13.5	15.7	2.2

Mean	(60)*	-10.3	-6.4	6.7	3.8	4.8	6.3
September	361-371	-39.6	-41.1	1.5	-3.3	-7.4	4.1
	400-411	-42.0	-39.8	2.2	-26.7	-24.6	2.1
	480-495	-19.5	-26.0	6.5	-16.1	-14.6	1.5
	500.5-508.5	-30.0	-25.9	4.1	-27.4	-23.2	4.2
	580-591.5	-16.3	-17.6	1.3	-9.5	-12.5	3
	829.5-835	-19.8	-18.8	1	9.9	10.7	0.8
	901-909	-10.4	-5.8	4.6	17.3	17.2	0.1
	927-935	-5.5	-4.7	0.8	4.6	5.1	0.5
	1003.5-1011	-3.9	-5.0	1.1	3.6	2.4	1.2
	1022.5-1027.5	-11.3	-13.3	2	-0.7	-2.3	1.6
	1144.5-1150	1.9	1.5	0.4	0.7	0.5	0.2
	1201-1209	-23.5	-23.4	0.1	13.8	13.9	0.1
	1240-1253	-30.3	-21.0	9.3	9.2	2.4	6.8
	1320-1327	-21.0	-23.1	2.1	20.6	18.7	1.9
Mean	(123)*	-21.3	-20.8	2.6	-2.2	-3.0	2.0

October	61.5-67.5	3.8	3.8	0.0	9.3	9.1	0.2
	80-85	-0.5	-0.5	0.0	0.2	0.7	0.5
	101.5-106.5	0.4	0.4	0.0	1.3	1.3	0.0
	120.5-131	5.2	5.5	0.3	5.8	5.7	0.1
	142-148.5	7.8	7.9	0.1	0.1	0.2	0.1
	160-165.2	12.2	12.4	0.2	0.6	0.8	0.2
	189.5-194.5	-10.4	-10.7	0.3	8.1	8.2	0.1
	205-210	5.4	5.5	0.1	-0.7	-0.5	0.2
	224-233	0.1	0.5	0.4	0.2	0.6	0.4
	242-253.5	-0.0	-0.1	0.1	-1.2	-1.3	0.1
	262-275	4.8	5.7	0.9	0.7	1.7	1.0
	282-295	5.8	6.2	0.4	-2.8	-2.4	0.4
	324.5-331	6.0	5.5	0.5	-4.0	-4.6	0.6
	342-355	4.4	5.5	1.1	-7.0	-6.9	0.1
Mean	(124.2)*	3.5	3.8	0.3	0.1	0.2	0.1

*(time) = total time included in time-weighted average

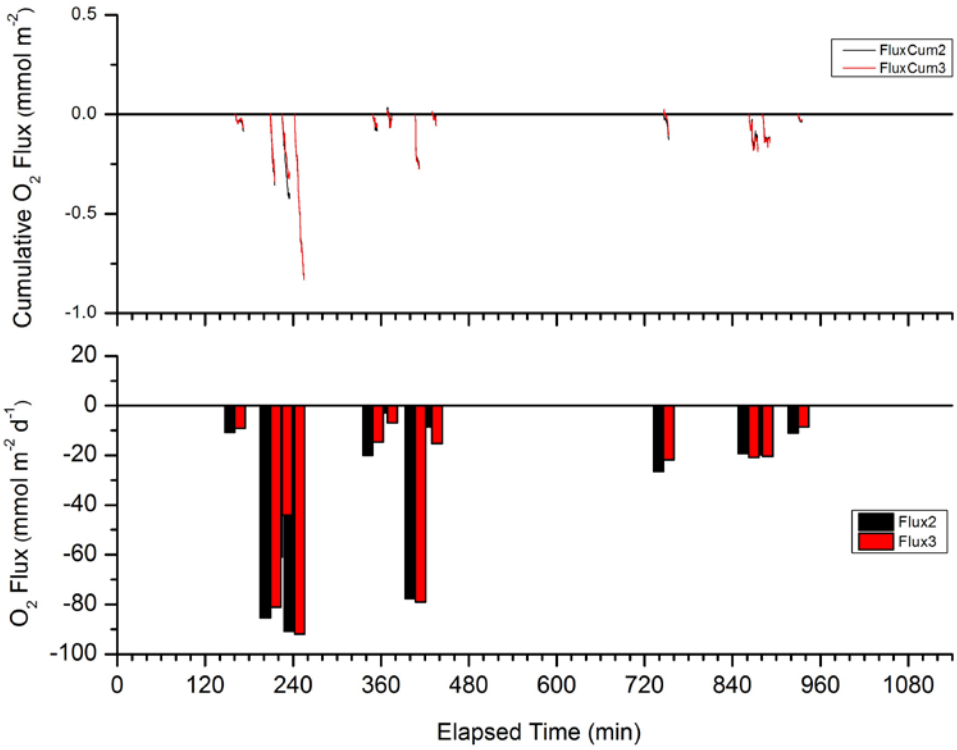

Figure 11 Cumulative O_2 flux (top) and derived O_2 flux (bottom) for 12 bursts in June. Mean O_2 uptake by sediments with flux 2 (linear) and flux 3 (running average) calculations = -36.2 and -34.5 mmol O_2 m^{-2} d^{-1}, respectively.

O_2 fluxes in July were smaller than June in general; in addition the July deployment took place mainly overnight and was during a period of little wave impact. Minimum O_2 uptake occurrence differed between flux 2 (-7.00 mmol m^{-2} d^{-1} at t=440, just before midnight) and flux 3 (-3.79 mmol m^{-2} d^{-1} at t=560, just after midnight) during July, while maximum O_2 uptake occurred during the same burst for flux 2 and 3 (-33.15 and -23.10 mmol m^{-2} d^{-1}) at t=300 (9pm) (Figure 12). Most of the cumulative flux calculations show nice linear progressions, which is an indication of a quasi-steady state, not surprising given the calm conditions (small current velocities and small waves), and the stable, though slowly decreasing bottom water O_2 in July.

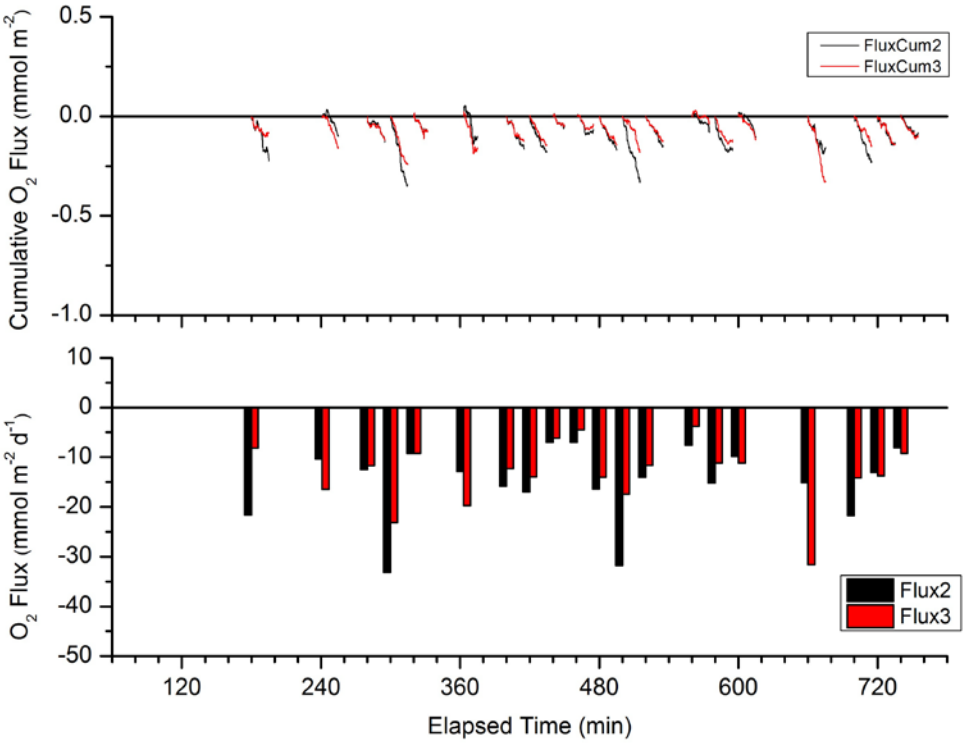

Figure 12 Cumulative O_2 flux (top) and derived O_2 flux (bottom) for 20 bursts in July. Mean O_2 uptake by sediments with flux 2 (linear) and flux 3 (running average) calculations = -15.77 and -13.99 mmol O_2 m^{-2} d^{-1}, respectively.

The August deployment also occurred overnight, but many of the bursts exhibited low frequency influences when examined individually with increasing N_r. Consequently, the five bursts accepted show unevenly progressing cumulative fluxes as well as divergent results between the flux 2 and flux 3 mean removal calculations (Figure 13). It is worth mentioning that vertical current velocities (V_z) were the strongest in August out of all the months, and again, August was one of the only months with very little change in horizontal current direction. September showed the same pattern as June with minimum O_2 uptake occurring in the early morning (positive fluxes of 1.86 and 1.49 mmol m^{-2} d^{-1}, flux 2 and flux 3 respectively) at t=1144 (~5am) and maximum O_2 uptake occurring in the early evening (-39.60 and -41.06 mmol m^{-2} d^{-1}, flux 2 and flux 3 respectively) at t=360 (4pm) (Figure 14). The time-weighted mean flux for all acceptable bursts in June, July, August, and September ranged between -37.49 and -35.69 mmol m^{-2} d^{-1} (flux 2 and 3), -15.23 and -13.26 mmol m^{-2} d^{-1} (flux 2 and 3), -10.28 and -6.34 mmol m^{-2} d^{-1} (flux 2 and 3), and -21.27 and -20.74 mmol m^{-2} d^{-1} (flux 2 and 3), respectively.

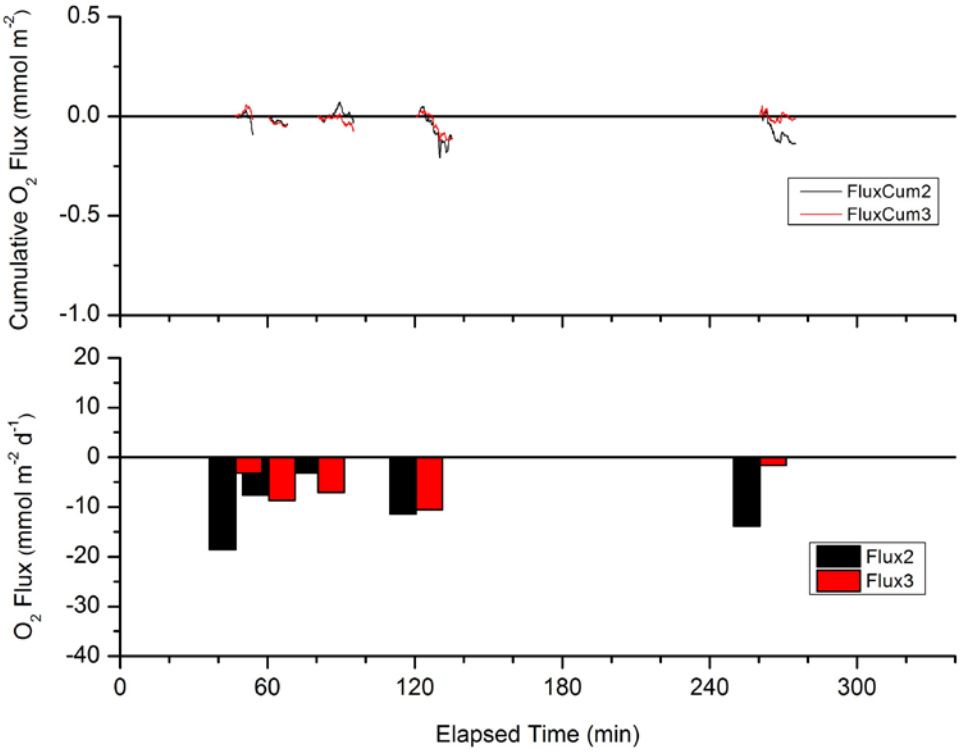

Figure 13 Cumulative O_2 flux (top) and derived O_2 flux (bottom) for five bursts in August. Mean O_2 uptake by sediments using flux 2 (linear) and flux 3 (running average) calculations = -10.91 and -6.23 mmol O_2 m^{-2} d^{-1}, respectively.

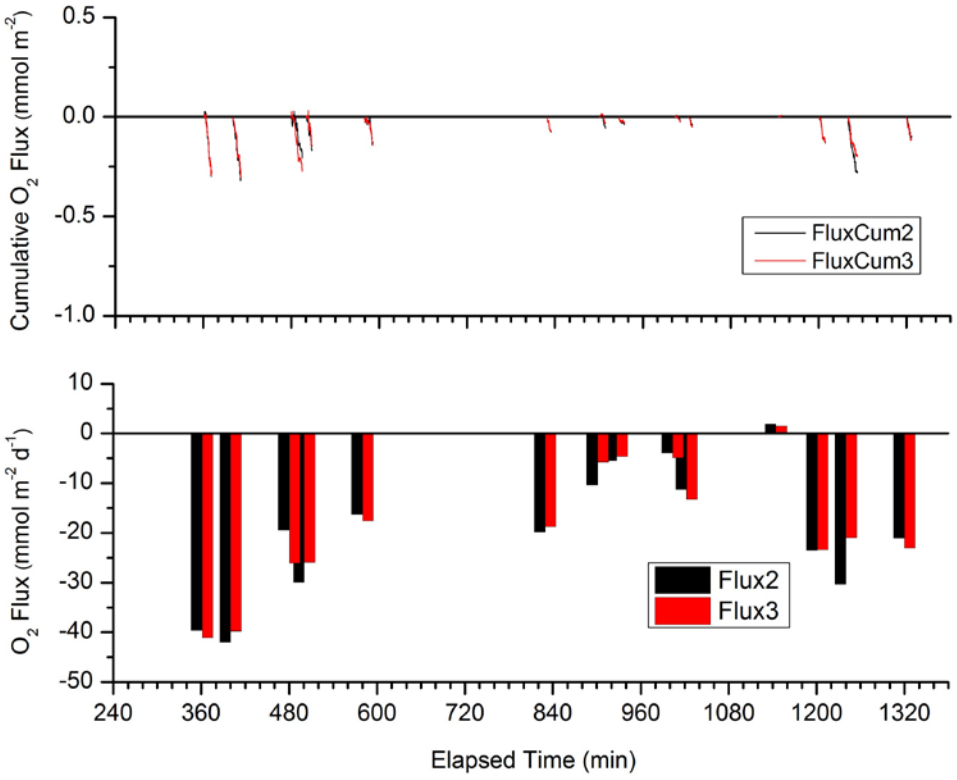

Figure 14 Cumulative O_2 flux (top) and derived O_2 flux (bottom) for 14 bursts in September. Mean O_2 uptake by sediments with flux 2 (linear) and flux 3 (running average) calculations = -19.36 and -18.83 mmol O_2 m^{-2} d^{-1}, respectively.

March and October both resulted in positive flux estimates suggesting O_2 production at the bed (see Table 2). However, rotating the March data (ranging from -216.0 to -208.9 degrees around the z-axis and -7.3 to -5.5 degrees around the y-axis) resulted in a large negative flux (flux 2: -85.9±43.1 mmol m^{-2} d^{-1}, flux 3: -84.2±42.7 mmol m^{-2} d^{-1}), and neither the unrotated nor rotated calculations agree well with an independent diffusive O_2 exchange rate of -3.4 mmol m^{-2} d^{-1} (see further results and discussion below). Rotating the October data (ranging from -40.7 to 79.2 degrees around the z-axis and -10.5 to -3.4 degrees around the y-axis) also gave a positive flux (see Table 2). Large, relatively persistent positive spikes throughout the O_2 microsensor data not removed by the MATLAB noise filter indicate that sand or zooplankton may have been hitting the electrode throughout the deployment, affecting its signal (Figure 15). This places the validity of the fluxes derived for October seriously in doubt.

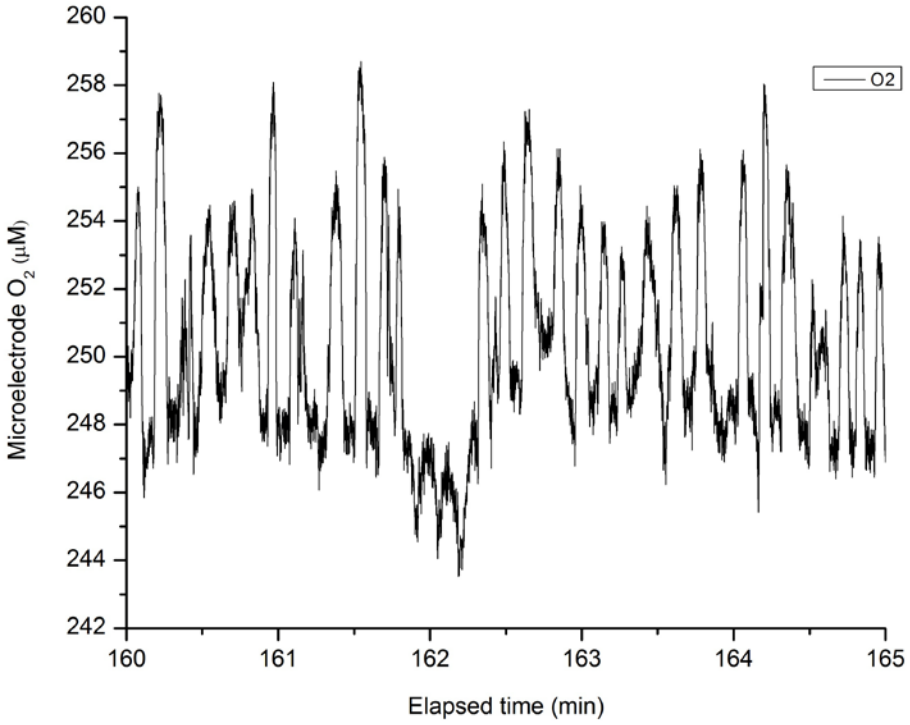

Figure 15 Five minutes of O_2 microelectrode data during the October deployment, illustrating spikes possibly caused by debris (sand or plankton) hitting the sensor. Since the spikes are not evenly distributed around the mean they would alter the flux calculation.

The horizontal current made large 180-360° changes during some deployments, for example June, but was nearly unidirectional in others, such as March. During our July deployment the current began in one direction and slowly migrated 180˚ then remained fairly constant for the remainder of the deployment (Figure 16). August was again nearly unidirectional (Figure 17), while in September the current direction changed somewhat continuously, and in October it slowly migrated in one direction. This is important to keep in mind given that currents affect advection, and consequently the transport of O_2 towards or away from the sensor location.

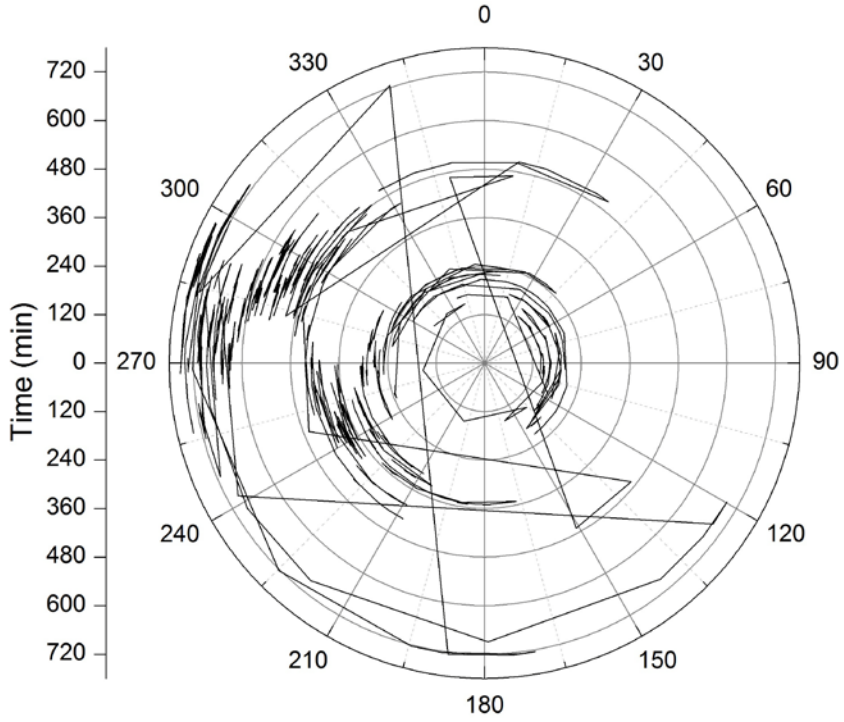

Figure 16 July horizontal current direction shows migration from ~ 90° to 270° during the deployment. Y-axis depicts time (min) and is represented in rings on the compass, beginning with time=0 at the center and moving outwards at 2-hour intervals.

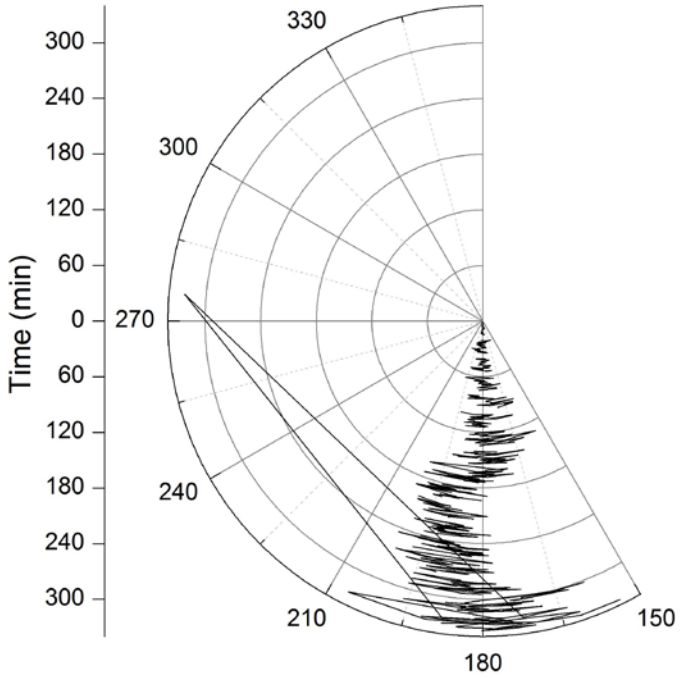

Figure 17 August horizontal current is very uni-directional, mainly staying between 165° and 195°. Y-axis depicts time (min) and is represented in rings on the compass, beginning with time=0 at the center. This was a shorter deployment than July and each ring represents only 1-hour.

Peaks at wave frequencies, as well as lower frequency turbulent eddies, can be seen in examples of the frequency cospectra calculated after removing means (using a running average with N=3601) from individual bursts for most months. A typical cospectrum for a burst in July shows no pronounced wave influence (Figure 18) while a typical cospectrum for a burst in September (Figure 19) shows a significant contribution to the flux from waves at a frequency of ~0.1Hz. The average wave period (T_p) derived from the bottom water pressure data in September was 10.52 s (Table 1), which gives a frequency of .095 Hz (1/p).

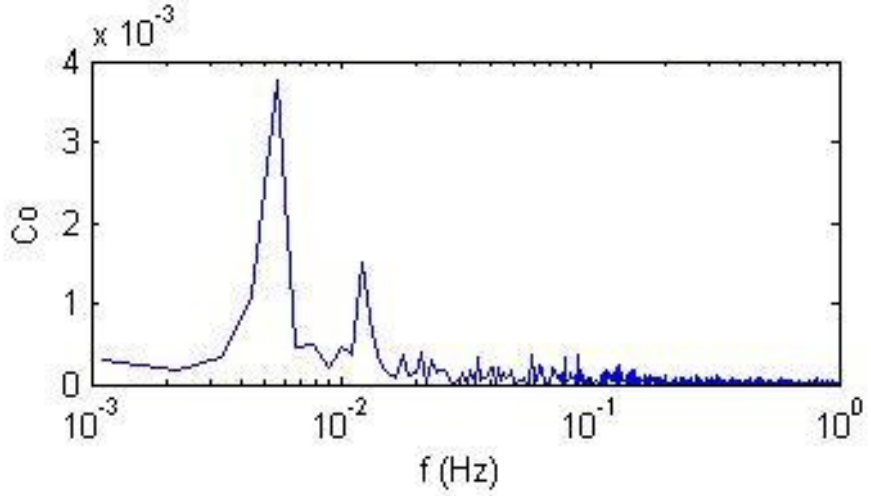

Figure 18 Cospectrum of $u_z'C'$ (x10^{-3} μmol cm^{-2} s^{-1}) for burst 21 in July illustrates strong contribution to O_2 flux by turbulent eddies in the .003 to .007 Hz frequency band.

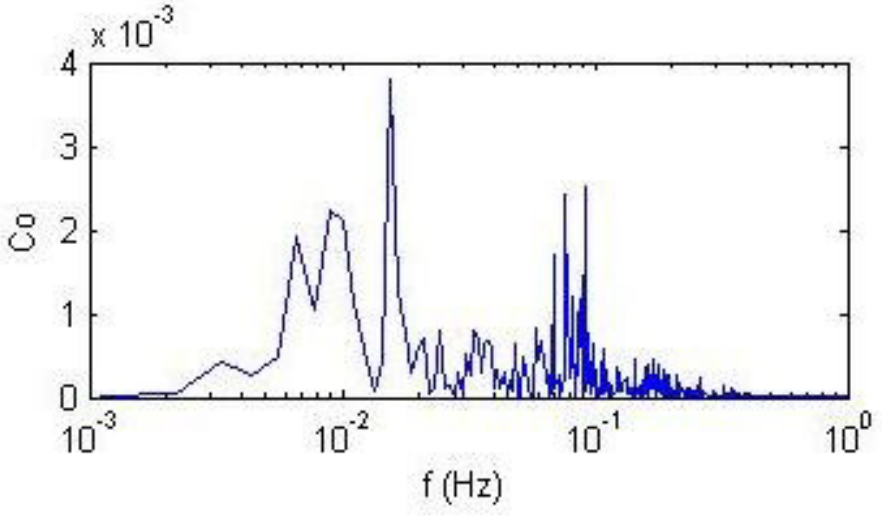

Figure 19 Cospectrum of $u_z'C'$ (x10^{-3} µmol cm^{-2} s^{-1}) for burst 19 in September illustrates a strong contribution to O_2 flux by wave influences (0.07-0.11 Hz band), as well as turbulent eddies (0.006-0.011 Hz band). The wave period in September averaged 10.52 s.

Sediments

Physical Properties

Sediment cores collected during the months of March, June, August, and October of 2009 all contained sandy sediments with variable amounts of shell fragments, including pieces of sand dollars; most cores also contained a minor amount of woody debris and small animals on occasion (polychaetes, amphipods, and gastropods). In the one core analyzed for grain-size down-core (Core B), sediments were well-sorted with a mean grain size of 174μm (SE=33 μm, March) for depth intervals of 0-17 cm, ranging from 101 μm (SE=114 μm, 15-17 cm) to 198 μm (SE=67 μm, 2-3 cm), and normal distributions. Composition was 100% sand at the surface (0-5 cm) with increasing silt and clay down the core (>5 cm) (maximum at 15-17 cm = 2.7% silt, 0.6% clay), though the amount of fines was extremely low in general (see Methods for explanation of fines).

Permeability (k) ranged from 1.3E-11 m^2 (SE=8.67E-14 m^2, March Core D, n=6) to 4.73E-11 m^2 (SE=3.88E-13, June Core H, n=4) (Figure 20), which falls within the documented range for sandy sediments (Burdige, 2006). Percent fines as determined by our quick settling and decantation method ranged from 0.4% (SE=0.1%, 0-5 cm, August Core F) to 1.9% (SE=0.5%, March Core C) (Figure 21). Average porosity (0-5cm) ranged from 0.26 (SE=0.030, June Core G, n=5) to 0.38 (SE=0.003, August Core J, n=5) (Figure 21) indicative of randomly packed, homogeneous, sphere-shaped particles. There was no temporal trend; however, there was a consistent decrease in porosity from 0-2 cm to deeper intervals in each core. In situ formation factor values for the sediment averaged 2.7 (Figure 22). Sediment resuspension and migration was evident in the ADV's Distance Check/Probe Check record. The change of sediment surface height ranged from 0.65±0.23 cm (March, max-min±SE, n=10) to 2.9±0.65 cm (October, n=32) (see Appendix A, Table A-2). The sediment microtopography was dominated by ripples but also showed evidence of bioturbation (Figures 23 and 24). Suspended sediment and camera focusing issues obscured photos of the bottom during some months.

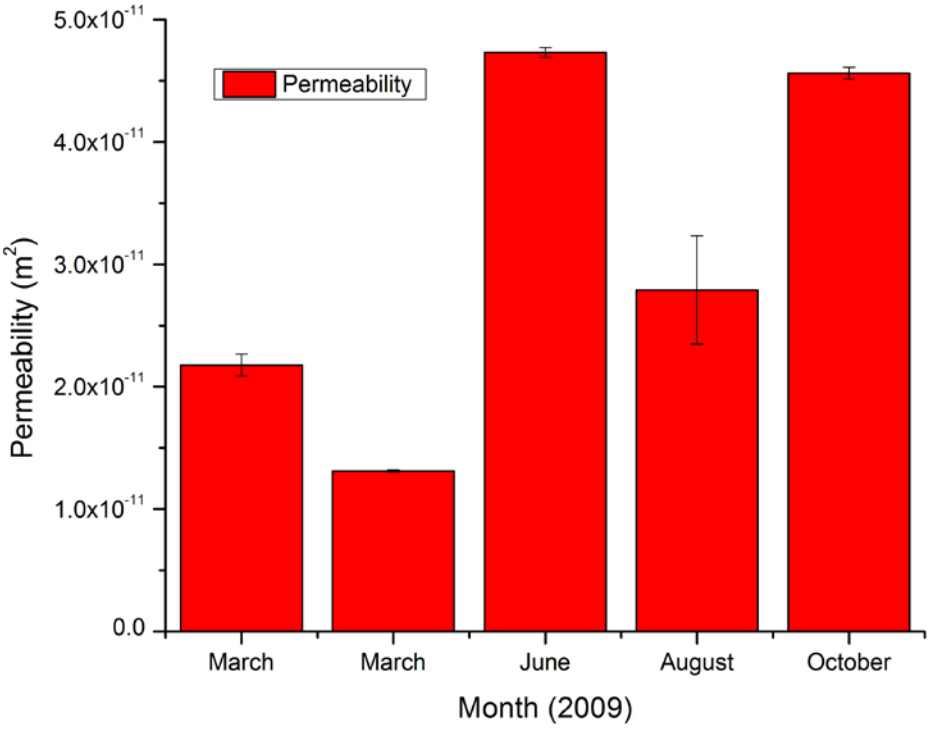

Figure 20 Mean permeability measurements by month, each error bar represents ±1SD from the mean. Two cores were measured in March, one core was measured in all other months.

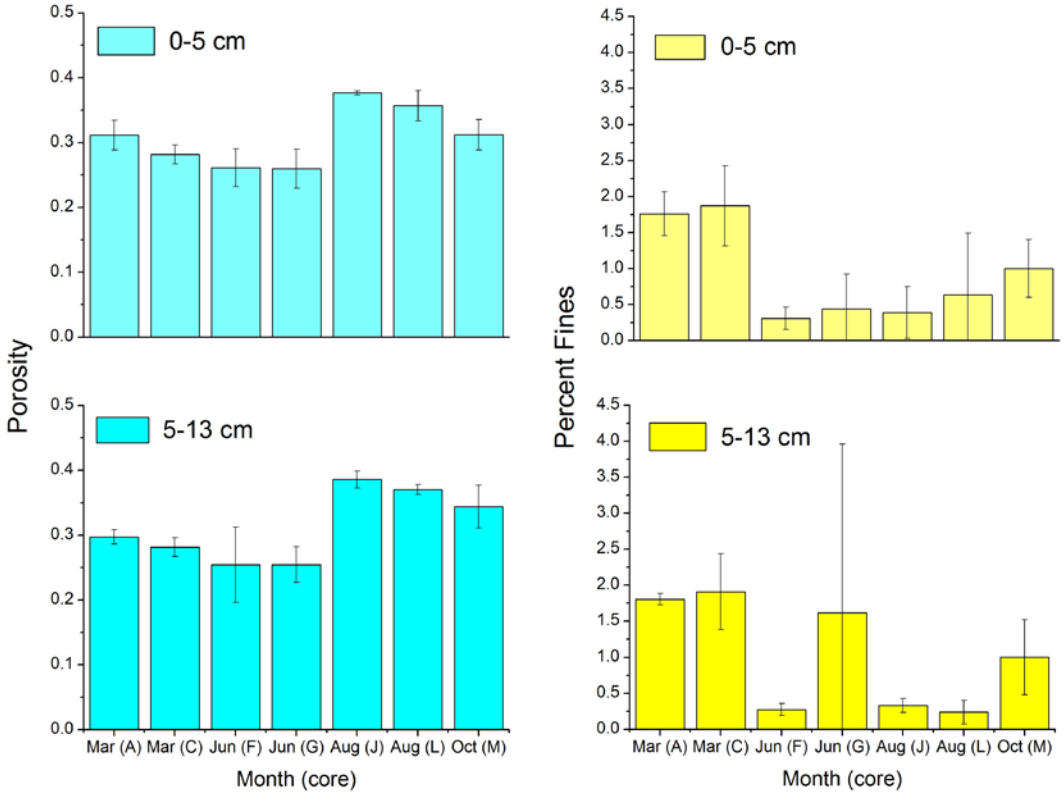

Figure 21 Average porosity (left) and average weight percent fines (right) for sediment layers 0-5 cm (top) and 5-13 cm (bottom). One core was sampled for October; all other months include two cores. Each error bar represents ±1SD from the mean.

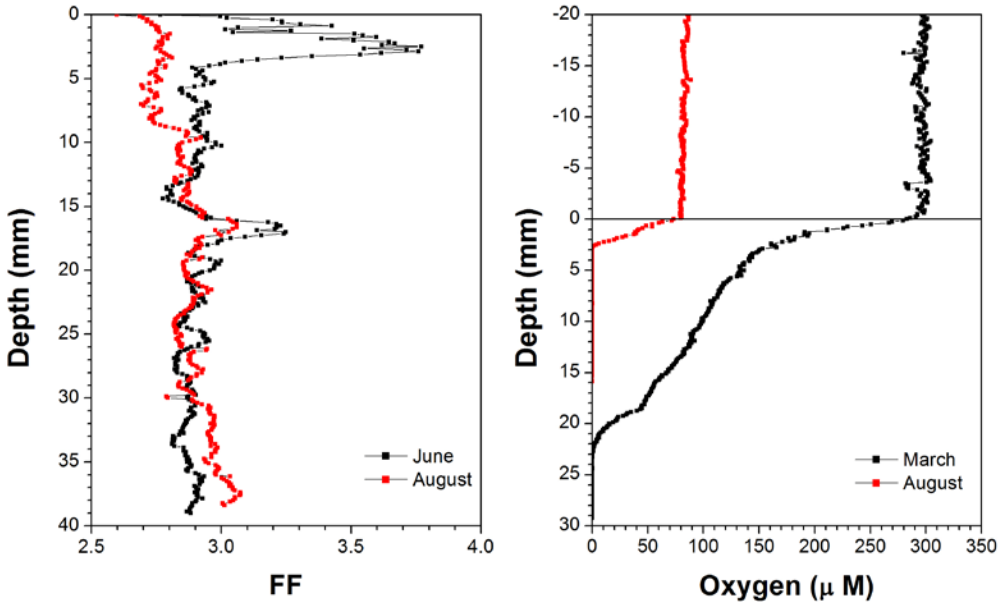

Figure 22 Sediment formation factor and O_2 profiles measured in situ. It appears the resistivity probe encountered a high resistance object such as a sand dollar or shell at the surface in June. Diffusive O_2 flux = -3.36 and -1.85 mmol m^{-2} d^{-1} for March and August, respectively.

Figure 23 Digital image of the seafloor next to the EC tripod in March 2009 depicts ripples and bioturbation, as well as shell fragments.

Figure 24 Digital image of the seafloor next to the EC tripod in March 2009 depicts bioturbation with gastropods and crustaceans visible, as well as shell fragments.

Biological Properties

Sediment pigment data was grouped into averages for the 0-5 cm and 5-13 cm intervals, by core (Figure 25). Individual intervals and concentrations of deeper intervals are given in Appendix B, Table B-2. In general, chlorophyll-α increased from spring through autumn. In all months the upper intervals (0-5 cm) contained higher concentrations of chlorophyll-α compared with the deeper intervals, but on the whole concentrations were very low, ranging from 0.03±0.03 μg g^{-1} (March, SE±mean, n=6) to 0.45±0.17 μg g^{-1} (October, n=6). Concentrations of phaeophytin-α also increased from March to October, ranging from 0.6±0.3 to 1.4±0.5 μg g^{-1} (March and October, respectively), and these concentrations are interpreted to reflect levels of degraded organic matter. Comparing whole cores (0-21cm), March contains the highest percent phaeophytin-α (95±2.9%) and August and October contain the lowest (69±2.1% and 75±3.5%, respectively), suggesting that over winter at this site nearly all of the fresh sedimentary organic material is degraded or swept away. Chlorophyll-α was mostly well-mixed down each core, with only a slight increase in the upper intervals (0-5 cm) when compared with lower intervals (5-13 cm). However, concentrations in surficial layers (0-1 cm) were considerably larger for most months. The surface layer for March (0-1 cm) contained a much higher amount of chlorophyll-α (0.13 μg g^{-1}) compared with remaining intervals down the core, producing a large SE for the 0-5 cm composite (Figure 25). Chlorophyll-α reproducibility of duplicates (rpd) values averaged 32.6, 12.0, 3.1, and 14.1% for

March, June, August, and October, respectively. The March rpd value was high due to one duplicate set at 3-4 cm (54.5%). Phaeophytin-α rpd values averaged 1.7, 2.9, 1.9, and 6.4% (March, June, August, and October, respectively).

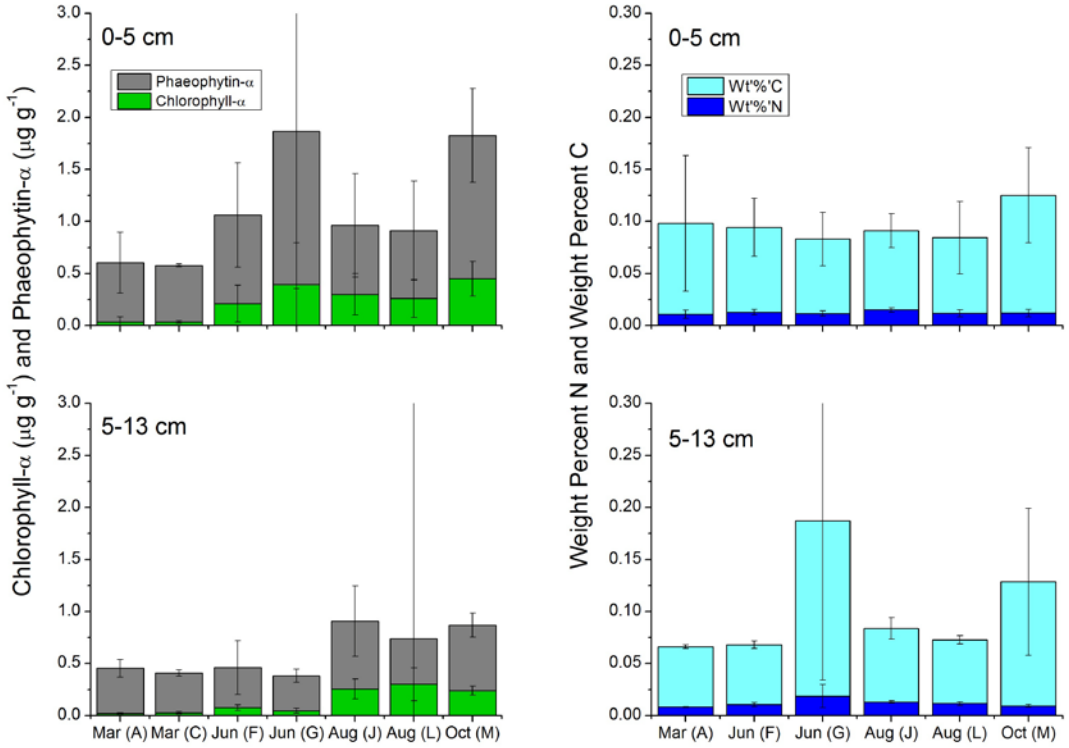

Figure 25 Average chlorophyll-α and phaeophytin-α concentrations (left) compared with average weight percent carbon and weight percent nitrogen (right) for sediment layers 0-5 cm (top) and 5-13 cm (bottom). Each error bar represents ±1SD from the mean.

Chemical Properties

The IMP deployments were successful and O_2 profiles were measured in March and August. One O_2 profile in March had a steep interfacial gradient from 0-1.4 mm and an O_2 penetration depth of 21 mm, signifying advective pore water transport that would contribute to the total flux and make diffusive flux estimates under-representations of the total O_2 utilization. Interfacial gradients from March and August indicate a diffusive O_2 flux of -3.4 and -1.9 mmol m^{-2} d^{-1} (respectively) when calculated using Fick's First Law of Diffusion as it is commonly applied to sediments, wherein the flux is assumed to be proportional to the concentration gradient (Burdige, 2006) (Figure 22). O_2 profiles were not successfully measured across the sediment-water interface for other months; in June the O_2 microelectrodes broke before reaching the sediment interface (possibly due to crabs or other organisms) and in October there was too much sediment movement to be able to detect stable profiles of either O_2 or formation factor.

C:N analysis was completed for all four months. Organic richness of the top 5 cm of sediment was very low: 0.09±0.07, 0.08±0.03, 0.07±0.03, and 0.11±0.05%OC (March, June, August, October, respectively) and 0.01±0.00%N (all months) (Figure 25). The C/N ratio was lowest in August (6.5±1.1) and highest in October (10.9±2.3). In most cases the samples were lower in carbon and nitrogen than the lowest standard. This may have introduced compound error into the C/N ratios.

Property Comparisons

Using interval or whole-core measurements (e.g. for permeability) from March, June, August, and October cores, there was a significant correlation between weight percent fines and weight percent carbon, $r(82)=0.61$, $p<.05$, as well as weight percent fines and permeability, $r(2)=0.44$, $p<.05$. There was no significant correlation between chlorophyll-α and weight percent carbon, $r(50)=0.24$, $p<.05$; chlorophyll-α and weight percent fines, $r(50)=0.22$, $p<.05$; or permeability and porosity, $r(2)=0.27$, $p<.05$.

DISCUSSION

Eddy Correlation Measurements

In this section we consider which EC fluxes are acceptable and which are not, as well as unique results that required special consideration. We also look at how O_2 fluxes and profile measurements on the Oregon shelf compare to other marine environments.

To begin, the positive fluxes found in both March and October are difficult to validate and may be attributed to methodological artifacts. Although some light does reach the seafloor at 30 m, evidence of benthic O_2 production is not found within in situ O_2 profiles, surface sediment chlorophyll-α concentrations, or the day-night variations seen in O_2 fluxes in other months. While our chlorophyll-α results showed a higher concentration in the surface layer for March, overall concentrations were especially low at this site and the upper sediment intervals (0-5 cm) were lower in March than all other months. This would not support the presence of active surface films of benthic algae and high rates of benthic O_2 production implied by the positive flux calculation. In comparison, Jahnke et al. (2000) measured high rates of benthic primary production for similar study sites at 14-40 m water depths in the South Atlantic Bight using transparent in situ benthic chamber deployments; however, high in situ PAR levels and high concentrations of chlorophyll-α in surface sediments did support their results. They also found that sediment resuspension events, as well as production in the water column, could greatly reduce benthic primary

production rates (e.g., from 824 mg C m^{-2} d^{-1} in August to 57 mg C m^{-2} d^{-1} after a storm in September)(Jahnke et al., 2000). If we were to sample over the winter months when water column production and turbidity may both decrease (in the absence of storms), it is possible that we would see benthic O_2 production if conditions were right (i.e., during a sunny day). Our March deployment was very short (it was our first trial of the EC equipment), giving only 60 minutes of data, and it was near dusk when light levels were low. The large differences between the rotated and unrotated flux calculations suggest both may carry biases stemming from horizontal or vertical advection or horizontal divergence of the turbulent flux. Thus, we are not prepared to accept either result without new supporting measurements or analyses that are beyond the scope of this study.

Similarly, after reviewing the October data, we feel confident that large spikes in the microelectrode data corrupted the flux calculation, causing a positive flux artifact. In Figure 15 the majority of spikes are positive, which would have caused the calculation to 'see' a false increase in O_2 concentration, thus resulting in a positive flux.

On the other hand, after conservative screening of data records for June, July, August and September, the O_2 fluxes derived for these months are believed to be reliable. Temporal shifts in the O_2 and temperature measurements during June, August, and September deployments suggest inhomogeneous water masses moving over our lander. Regardless, a majority of the cumulative flux calculations for the months of June and September show strong linear progressions. During

the second high tide in June (t=860 min) two bursts show uneven progress at the end, indicating a low frequency eddy contributing to the flux that was not captured during the time allotted for the burst period. Interestingly, graphing these bursts with increasing N_r (see Methods) did not indicate such influences (Figure 11, bursts 44 and 45). The September data shows strong currents throughout the deployment with large changes in velocity during the middle of the deployment (Figure 10) and most bursts had to be eliminated from this section. Still, many successful flux derivations were possible for other portions of the deployment, showing strong, linearly progressing cumulative fluxes that correlate well between the flux 2 and flux 3 mean removal calculations.

However, the August flux results showed a low frequency influence throughout the deployment that was not accommodated by our sampling or data processing methods. Upon graphing increasing N_r (data not shown) most of the bursts did not reach a near-constant O_2 flux but either continued to increase or decrease substantially, or show an obvious oscillating pattern, strongly indicating that we needed a longer sampling time to capture all eddies contributing to the flux during this month. August did have the strongest vertical velocity (v_z), as well as the largest resultant of the mean x, y, and z velocities out of all months sampled. This may have introduced a horizontal advective influence causing a breakdown of our methods (see assumptions in Methods). In the future, it may be advisable to sample continuously without rest periods so that all contributing eddy sizes can be captured during the sampling period.

The EC microelectrode data in July had a relatively noisy signal that can be seen in Figure 8 (O_2 data), but these high frequency variations contributed very little to the overall flux, as is illustrated by Figure 18.

EC results for accepted data after processing show that O_2 flux varies between -6.2 and -30.7 mmol m^{-2} d^{-1} (June-September using the running average mean removal method with N_r=3601), which compares well with other in situ measurements of benthic respiration rates in similar environments (-10 to -40 mmol m^{-2} d^{-1}) (Glud, 2008; Reimers et al., 2004). Compared to chamber flux measurements on the Washington shelf at water depths between 85 and 185 m, our results indicate slightly greater rates of O_2 uptake. The Washington shelf O_2 fluxes ranged from -4.7 to -18.6 mmol m^{-2} d^{-1} (Archer and Devol, 1992). Our EC fluxes are also consistent with the findings in 52 studies that Glud (2008) compiled from a wide range of locations using traditional methods for measuring O_2 consumption. Glud (2008) showed that O_2 consumption averages ~-25 mmol m^{-2} d^{-1} at most 30 m sites and consumption rates decline sharply with water depth.

As EC is a new method for benthic studies there are no published results of EC fluxes from similar sites available. However, one study conducted overnight at an intertidal bay in water depths of 1-1.5 m (with benthic photosynthesis occurring during the day) showed O_2 flux rates much larger than our measurements, ranging from approximately -1500 to 400 mmol m^{-2} d^{-1} (Berg and Huettel, 2008). Another study conducted at an intertidal sand flat in water depths

<0.69 m with benthic photosynthesis and almost 100% air-saturated water also showed O_2 flux rates larger than our measurements, ranging from -14.5 to 6.6 mmol O_2 m^{-2} h^{-1} (-348 to 158 mmol O_2 m^{-2} d^{-1}) (measurements made during both night and day) (Kuwae et al., 2006).

Microprofile data on the Oregon shelf in March resulted in an O_2 penetration depth of ~21 mm, comparable to results from other studies in wave-impacted permeable sediments with high turnover rates. One study conducted in the North Sea found O_2 penetration depths between 0.5 and 45 mm for water depths of 25 to 58 m, depending on the time of year (Lohse et al., 1996). O_2 penetration depth on the Oregon shelf is also variable. Contrast the March microprofile with August, which had an O_2 penetration depth of only ~3 mm. Our EC measurements indicate that bottom water O_2 concentration in March was almost air-saturated (between 293 and 297 μM), while in August it was approaching hypoxia (between 101 and 159 μM). It appears anaerobic respiration may occur in subsurface sediments off Yaquina Head more intensely during the summer given that O_2 penetration was so shallow in August. Since O_2 consumption is caused not only by aerobic respiration, but also by the oxidation of reduced products, anaerobic respiration in the sediments may also contribute to intensification of the O_2 consumption rate.

Overlying water concentration can control O_2 penetration depth and therefore affect diffusive rates of O_2 uptake in sediments (Archer and Devol, 1992; Cai and Reimers, 1995; Cai and Sayles, 1996). Bottom water O_2

concentration has been shown to affect total O_2 flux as well. As part of a modeling study of biogeochemical processes on the Louisiana shelf (a human-induced hypoxic zone), Morse and Eldridge (2007) demonstrated that during hypoxic conditions O_2 flux is likely only ~20% of the flux that occurs during normal oxic conditions. Our EC flux measurements suggest this relationship between bottom water O_2 concentration and O_2 uptake even for organic-poor sediments. As previously stated, bottom water O_2 concentration was the lowest in August, averaging 125 μM, while EC flux measurements in August also resulted in the lowest O_2 uptake, averaging -6.2 mmol m^{-2} d^{-1}. By contrast, bottom water O_2 concentration was the highest in June (averaging 194 μmol) and EC flux measurements also resulted in the highest O_2 uptake during June (averaging -35.7 mmol m^{-2} d^{-1}). This pattern occurs throughout our results (Figure 26) and confirms previous studies indicating a relationship between bottom water O_2 concentration and flux.

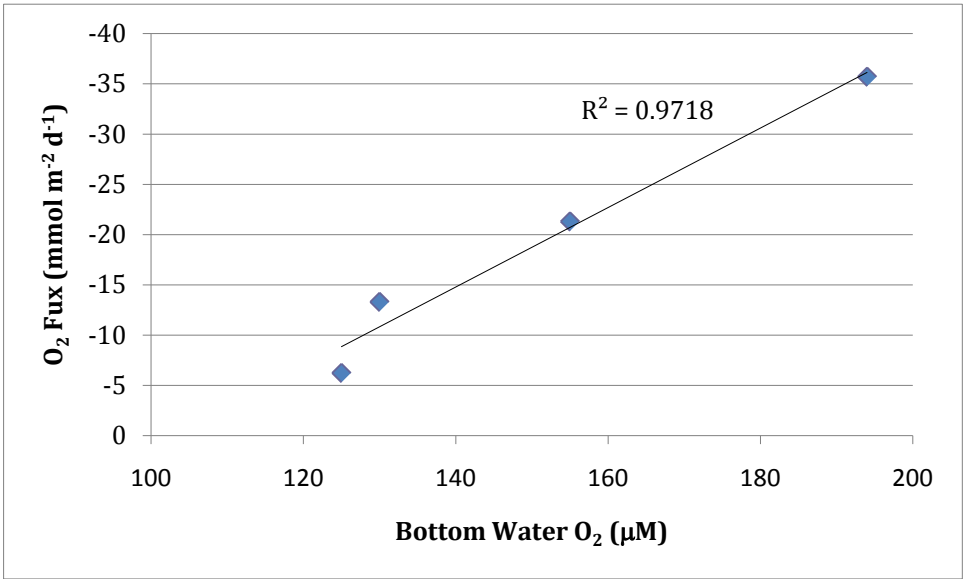

Figure 26 Average EC O_2 flux versus average overlying water O_2 concentration June-September 2009.

Inner Shelf Benthic Environment

In this section we consider the affects of waves and resuspension events on benthic O_2 consumption and production, as well as on the temporal and spatial variability of organic matter accumulation, in this highly energetic environment.

The physical dynamics of the inner shelf posed several challenges in measuring O_2 flux; in addition to a semi-diurnal tidal influence, high-energy currents and surface waves affect the seafloor off Yaquina Head. Short-term variations due to strong currents and periods of abruptly changing current velocities can combine with topographic features to redirect alongshore-coastal jets (Barth et al., 2005). The influences of these forces are visible in velocity and pressure records. Shallow-water waves can impact benthic O_2 consumption by increasing exposure of buried organic matter to oxygenated waters through advective pore water flow (Jahnke et al., 2000; Huettel et al., 2003; Reimers et al., 2004; Franke et al., 2006; Rusch et al., 2006). Increased O_2 flux from the pumping action of waves is demonstrated during measurements coinciding with larger waves, as illustrated in the 1-sided cospectrum from September (Figure 19). McGinnis et al. (2008) also demonstrated the contribution of waves to O_2 flux in their study using the EC method in a shallow water reservoir with basin-scale waves. Measurements were taken at ~3 m water depth and spectral plots show that surface and internal seiches contribute to O_2 flux (McGinnis et al., 2008). Visible ripples and near-bottom turbidity on the Oregon inner shelf, as shown in digital photos and transmissometry profiles (sensor data from CTD casts not

reported), support the conclusion that high turbulence and near-bottom oscillatory motions strongly affect this site, which we believe to be a major factor in O_2 exchange at this location (Huettel et al., 1996, 1998; Precht et al., 2004; Janssen, Huettel, et al., 2005; Franke et al., 2006).

It's reasonable to believe that wave-induced particle resuspension increases exchange between seawater and pore water, increasing rates of O_2 consumption at this site (Precht and Huettel, 2003; Reimers et al., 2004; Almroth et al., 2009). The high turbidity most likely limited light from reaching the seafloor, and benthic photosynthesis was not occurring regularly. This assumption is also supported by the fact that we found no evidence of benthic production in the microprofiles, and sediments were organically poor but contained a high percentage of phaeophytin-α, a degradation product of phytoplankton chlorophyll-α. Therefore, the seafloor is a locus for O_2 consumption on the Oregon inner shelf mainly through the decomposition of pelagic organic matter not organic matter produced at the sediment-surface.

Generally, studies of benthic-pelagic coupling have shown that an influx of nutrients into the water column (occurring in the spring) increases phytoplankton production, which as a result fuels zooplankton production, continuing throughout the food-web (Graf et al., 1983; Hill and Wheeler, 2002; Hales et al., 2006; Barth et al., 2007). Organic matter settling out from spring blooms onto the seafloor can show seasonal patterns; however, one study hypothesized that there is often a discrepancy between the water column and

sedimentation measurements due to resuspension and advection events (Hansen and Josefson, 2003).

Temporal and spatial variations were seen in the physical properties of sediment samples from the Oregon shelf as well as in the sediment pigment and CN data. These variations can be attributed to high incidence of particulate resuspension as well as particle settling to the seafloor between physical events (i.e. when seas are calm). There was a slight enrichment in carbon and pigment concentrations as well as percent fines for the upper sediment layers (0-5 cm) when examined as a whole, though as previously stated, all concentrations were very low so gradient recognition is difficult. Greater chlorophyll-α concentrations throughout the 0-5 cm intervals in summer agrees with Hansen and Josefson's (2003) hypothesis and suggests that the small amount of material making it to the seafloor is continually being mixed into the sediments and quickly remineralized on the Oregon shelf. Alternatively, detritus "snow" is remaining largely suspended in the water column and is then being advected off the shelf (Walsh et al., 1981).

Pb^{210} analyses were done for near surface intervals on our core samples (results not shown) and concentrations were so low that a sedimentation rate could not be derived, indicating that these sediments are predominantly relic and frequently winnowed of fine materials. One study of the Oregon shelf by Hales et al. (2006) found that O_2 and POC budgets in the water column do not balance, and they concluded that a majority of production is remaining suspended in the water

column and is then being exported off the shelf when seasonal upwelling relaxes in the fall. This scenario helps to explain why inner shelf sediment samples are so organically poor.

CONCLUSION

The upwelling season occurred from mid-May to mid-October on the Oregon shelf in 2009 (Pierce and Barth, 2010) and bottom water O_2 concentrations below air saturation are reflected during upwelling months in the EC measurements made six times between late March and late October. Climate variability and hypoxia on the Oregon shelf have become a growing concern due to recent regional occurrences of very low O_2 concentrations, and research is being done to better understand O_2 deficits in shelf waters (Bograd et al., 2008; Chan et al., 2008). A regional hub for the Ocean Observatories Initiative is scheduled for installation off the coast of Newport in the near future to help track changes in this nearshore environment. EC measurements may, with further development, be suitable for observatory measurements and provide long continuous records of benthic O_2 flux change in response to environmental forcing.

Through short EC time series, we gathered evidence that O_2 flux is strongly driven by bottom water O_2 concentration as well as physical forcing events, mainly bottom stress caused by waves and currents. The EC O_2 fluxes were comparable to fluxes derived from other methods used in similar environments. Thus, EC appears to be a valuable and accurate way to measure O_2 flux at wave-impacted sites.

We also observed higher pigment concentrations in the sediments for cores sampled during the summer compared to cores in March, but no clear

seasonal pattern in other sediment properties, or evidence for benthic primary production. Furthermore, the overall low pigment and carbon concentrations suggest that much of the primary production occurring in the water column is being exported off the shelf, and the small amount of organic material that does settle and become entrained in the sediments is remineralized rapidly. It is likely that oscillatory motion and pressure gradients associated with waves drive episodes of advective pore water exchange and ripple migration at the study site. This was apparent from the dominant frequencies in EC cospectra, O_2 penetration depths, acoustically measured changes in the sediment height, and benthic photographs.

In conclusion, this work demonstrates that EC flux measurements can be made at temporally diverse sites such as the Oregon shelf, and strong currents and large waves can be accommodated with some modification to original data reduction methods. The measurements made in 2009 form a baseline to document environmental changes in the future. More measurements of this kind at several depths and N-S locations are necessary in order to ascertain important interactions between the benthic and pelagic environments on the Oregon shelf.

APPENDICES

Appendix A

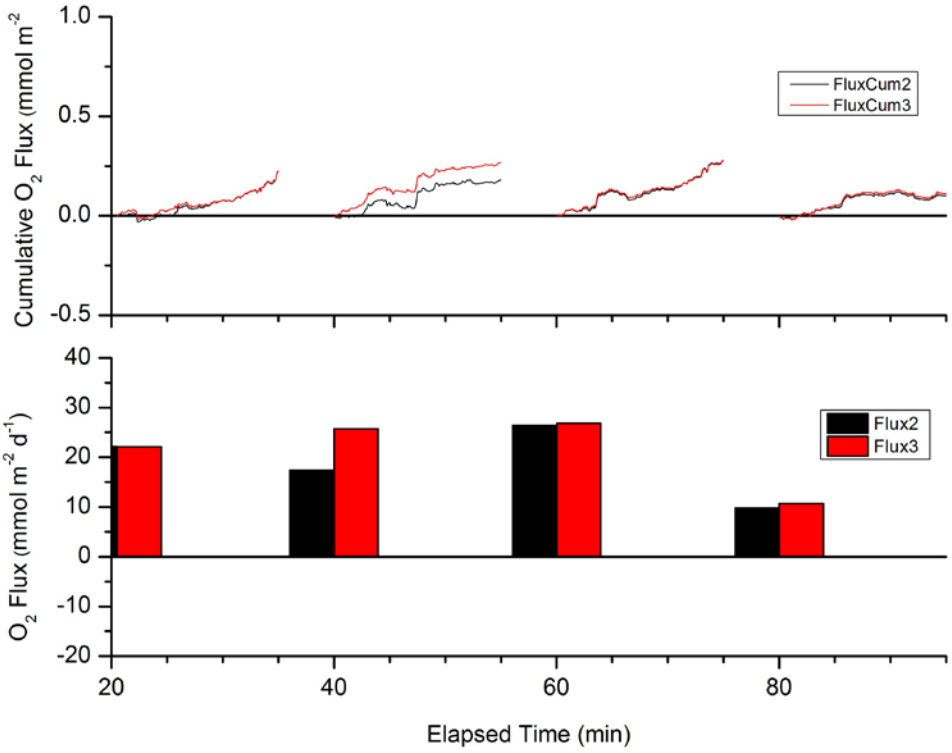

Figure A-1 Cumulative O_2 flux (top) and derived O_2 flux (bottom) for four consecutive 15-minute bursts in March. Mean O_2 flux of sediments using flux 2 (linear) and flux 3 (running average) calculations = 18.93 and 21.34 mmol O_2 m^{-2} d^{-1}, respectively.

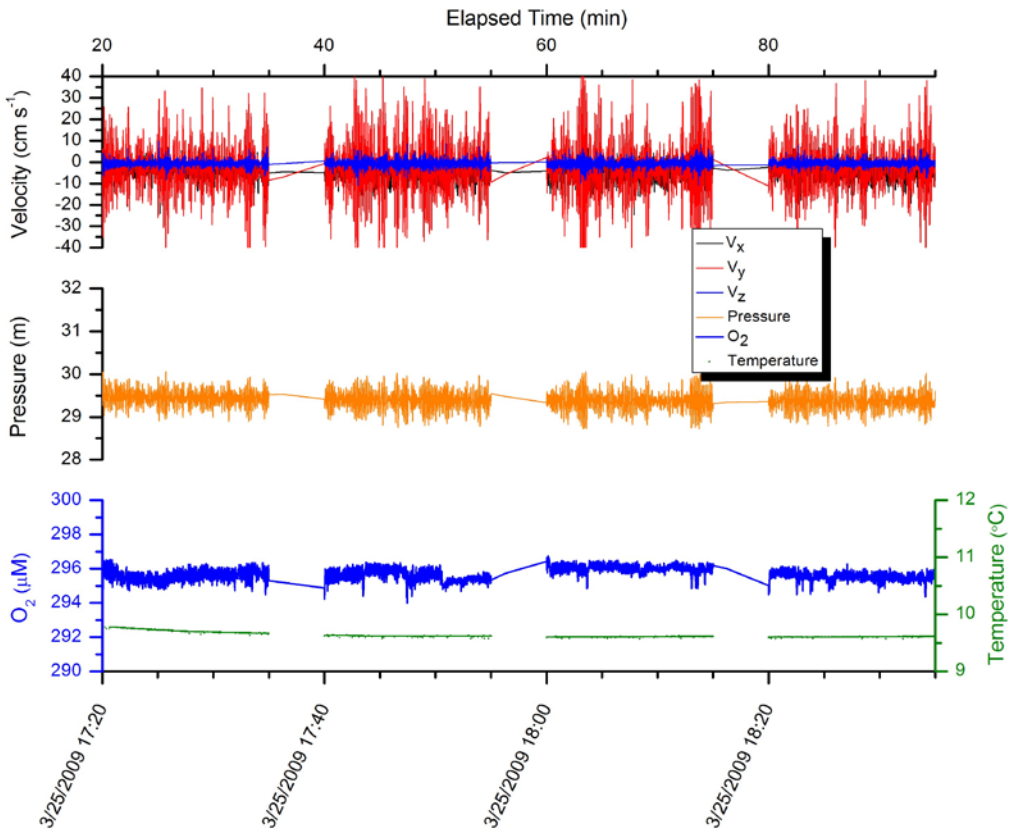

Figure A-2 Despiked 16-Hz velocity data (x, y, z) (top), pressure data (middle), and O_2 microelectrode and temperature data (bottom) for the same four consecutive, 15-minute bursts as shown in Figure A-1. Upper x-axis depicts time elapsed from instrument start time; lower x-axis depicts date and time.

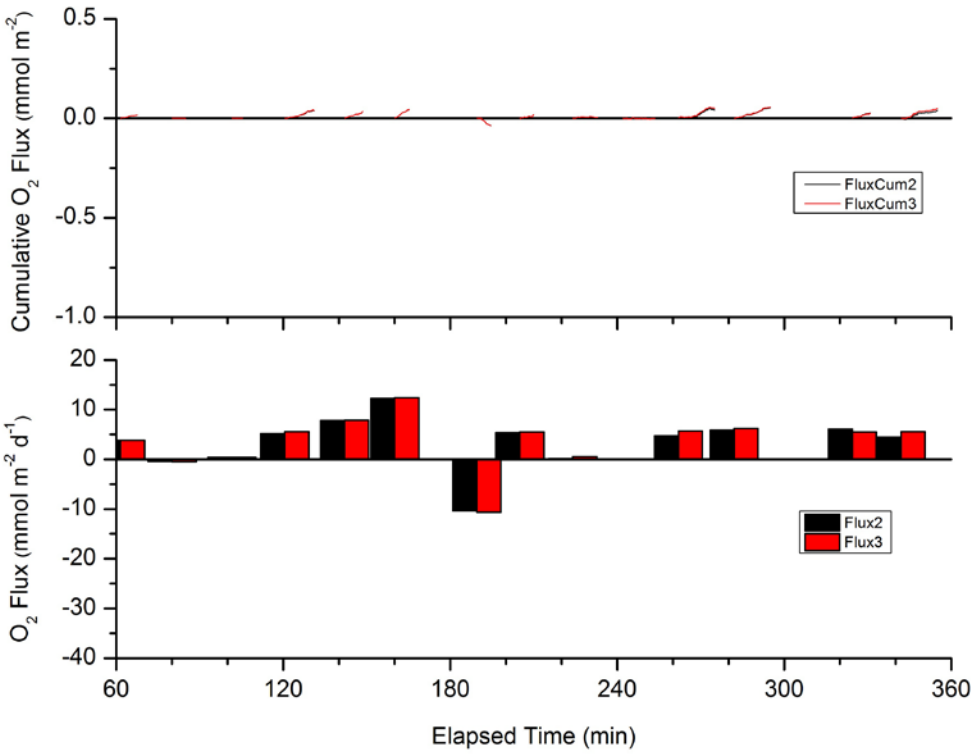

Figure A-3 Cumulative O_2 flux (top) and derived O_2 flux (bottom) for twelve bursts in October. Mean O_2 flux of sediments using flux 2 (linear) and flux 3 (running average) calculations = 3.21 and 3.40 mmol O_2 m^{-2} d^{-1}, respectively.

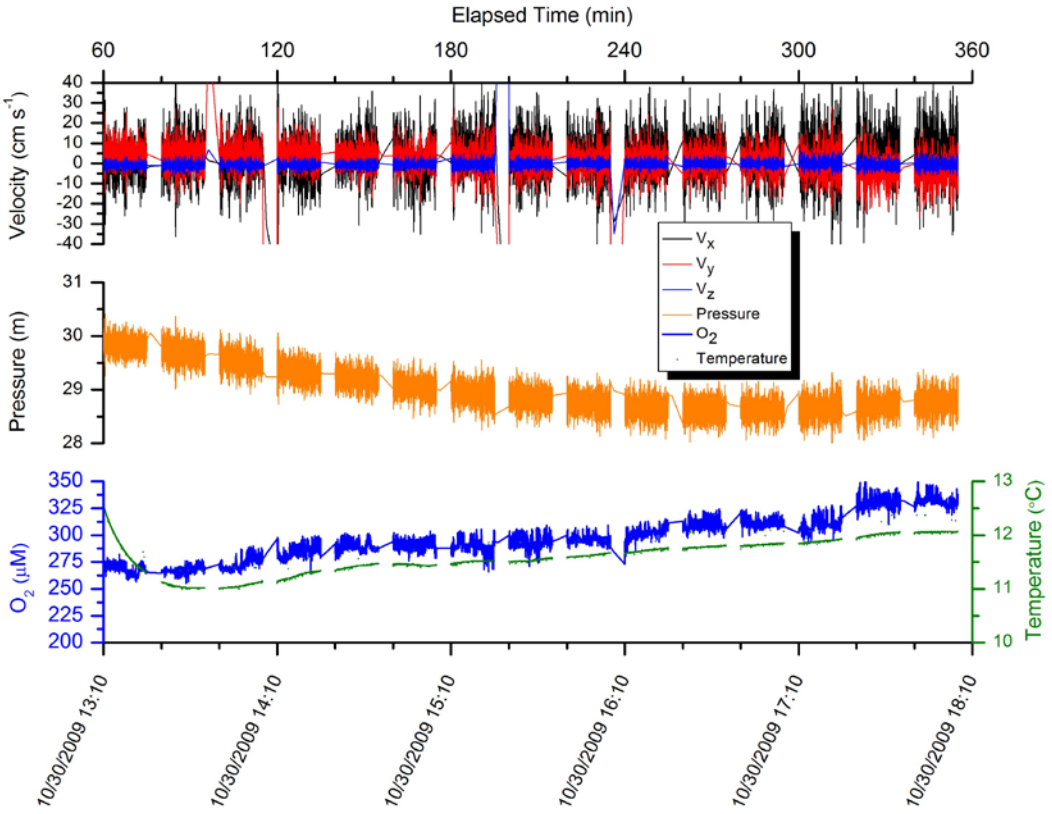

Figure A-4 Despiked 16-Hz velocity data (x, y, z) (top), pressure data (middle), and O_2 microelectrode and temperature data (bottom) for the same deployment time as shown in figure A-3. Upper x-axis depicts time elapsed from instrument start time; lower x-axis depicts date and time

Table A-1 Microelectrode sensor details, including measurements used for 2-point calibrations.

Cruise	Date	Event	Sensor	Tip Diameter (μm)	Na-Ascorbate Zero (pA)	Air Saturated Seawater (pA)	Hours Polarized
March W0903B	03/25/09	32	7557	8-12	016	173	82
March W0903B	03/25/09	44	J	9	015	248	72
April	04/28/09	1	R	6	003	116	48
June W0906A	06/10/09	41	8221	8-12	003	--	20
July	07/13/09	1	8259	20-30	017	122	5
August W0908A	08/19/09	46	8475	20-30	008	078	48
September	09/23/09	1	AL	4	005	--	3
October W0910B	10/27/09	1	8686	8-12	012	327	10
October W0910B	10/30/09	40	8666	8-12	006	--	22

--no data

Table A-2 Change in sediment surface height, calculated from the Vector .pck files as an average of the distance to the boundary for all three receiver signals, per burst.

Month	Minimum (cm)	Maximum (cm)	Difference (cm)	Standard Deviation	n
March	11.66	12.89	1.23	0.32	30
April	19.15	20.09	0.94	0.19	57
June	11.69	18.20	6.51	1.03	336
July	13.99	17.25	3.26	0.74	216
September	13.34	17.95	4.61	0.66	345
October	10.56	17.34	6.78	0.96	96

Appendix B

Table B-1 Physical properties of sediment cores.

Date	Event	Core	Location Lat. N	Location Long. W	Water Depth (m)	Core Length (cm)	Grain Size (μm)	Permeability (m^2)
3/25/2009	36	A	44 41.191	124 05.989	30	23	--	--
3/25/2009	39	B	44 41.183	124 05.972	30	--	174	2.178E-11
3/25/2009	40	C	44 41.180	124 05.982	30	55	--	--
3/25/2009	43	D	44 41.989	124 05.989	30	--	--	1.311E-11
6/10/2009	43	E	44 40.832	124 05.919	29.4	--	--	--
6/10/2009	45	F	44 40.830	124 05.930	30	29	--	--
6/10/2009	46	G	44 40.808	124 05.930	30	24	--	--
6/10/2009	47	H	44 40.809	124 04.946	30.7	--	--	4.733E-11
8/19/2009	36	I	44 40.820	124 05.890	30	--	--	2.792E-11
8/19/2009	39	J	44 40.831	124 05.885	30	27	--	--
8/19/2009	40	K	44 40.833	124 05.887	30	--	--	--
8/19/2009	42	L	44 40.847	124 05.895	30	46	--	--
10/28/2009	5	M	44 40.839	124 05.901	30	--	--	--
10/28/2009	44	N	44 41.126	124 05.918	29	--	--	4.563E-11

-- no data

Table B-2 Biochemical properties of sediments.

Date	Core	Depth (cm)	wt% fines	Chl conc (μg g^{-1})	Phaeo conc (μg g^{-1})	TN (wt%)	TOC (wt%)	C/N (mol/mol)
3/25/2009	A	0-1	1.670	0.135	1.160	0.018	0.204	13.49
		1-2	1.645	0.007	0.488	0.009	0.061	7.55
		2-3	1.936	0.010	0.490	0.009	0.059	7.85
		3-4	2.176	0.021	0.423	0.009	0.057	7.36
		4-5	1.379	0.010	0.427	0.008	0.057	7.88
		5-7	1.804	0.023	0.404	0.009	0.059	7.98
		7-9	1.750	0.014	0.374	0.008	0.058	8.61
		9-11	1.921	0.014	0.394	0.008	0.060	9.18
		11-13	1.751	0.027	0.561	0.008	0.056	7.71
		15-17	1.798	0.024	0.499	0.007	0.055	9.13
		21-23	2.034	0.016	0.309	0.007	0.056	9.50
3/25/2009	C	0-1	2.395	0.040	0.549	--	--	--
		1-2	1.747	0.042	0.546	--	--	--
		2-3	1.190	0.037	0.554	--	--	--
		3-4	1.546	0.008	0.516	--	--	--
		4-5	2.485	0.044	0.535	--	--	--
		5-7	1.583	0.031	0.406	--	--	--
		7-9	2.651	0.015	0.351	--	--	--
		9-11	1.488	0.020	0.360	--	--	--
		11-13	1.913	0.042	0.405	--	--	--
		15-17	1.796	0.045	0.582	--	--	--
		21-23	2.766	0.053	0.570	--	--	--
		27-29	3.093	0.019	0.340	--	--	--

6/10/2009	F	0-1	0.396	0.505	1.539	0.012	0.065	6.53
		1-2	0.239	0.061	0.429	0.011	0.062	6.41
		2-3	0.543	0.327	1.417	0.017	0.087	5.86
		3-4	0.199	0.191	0.768	0.011	0.066	6.93
		4-5	0.170	0.122	0.519	0.011	0.128	13.14
		5-7	0.173	0.115	0.763	0.011	0.059	6.48
		7-9	0.240	0.070	0.208	0.013	0.061	5.37
		9-11	0.323	0.057	0.219	0.069	0.058	6.95
		11-13	0.361	0.063	0.348	0.009	0.052	7.03
		15-17	0.332	0.077	0.400	0.014	0.057	4.79
		21-23	2.580	0.162	0.818	0.016	0.123	8.71
		27-29	1.004	0.043	0.193	0.009	0.053	7.22
6/10/2009	G	0-1	0.548	0.905	3.410	0.016	0.117	8.64
		1-2	1.243	0.204	0.710	0.011	0.065	7.01
		2-3	0.162	0.204	0.608	0.010	0.056	6.41
		3-4	0.119	0.083	0.361	0.010	0.059	6.86
		4-5	0.125	0.063	0.323	0.011	0.059	6.45
		5-7	0.115	0.060	0.321	0.011	0.062	6.65
		7-9	0.478	0.066	0.332	0.011	0.061	6.63
		9-11	0.762	0.015	0.421	0.018	0.164	10.44
		11-13	5.110	0.041	0.270	0.034	0.386	13.07
		15-17	1.098	0.071	0.398	0.009	0.064	8.04
		21-23	1.086	0.077	0.518	0.008	0.058	8.05
8/19/2009	J	0-1	1.028	0.338	0.751	0.017	0.100	6.90
		1-2	0.266	0.147	0.294	0.017	0.087	5.82
		2-3	0.225	0.144	0.294	0.012	0.067	6.39
		3-4	0.151	0.170	0.322	0.014	0.063	5.34
		4-5	0.288	0.663	1.572	0.014	0.064	5.25

		5-7	0.370	0.264	0.543	0.012	0.067	6.35
		7-9	0.366	0.184	0.490	0.012	0.057	5.70
		9-11	0.185	0.184	0.417	0.014	0.078	6.55
		11-13	0.393	0.390	1.152	0.014	0.079	6.60
		15-17	0.133	--	--	0.010	0.059	7.15
		21-23	0.474	0.143	0.373	0.012	0.067	6.65
8/19/2009	L	0-1	2.156	0.497	1.265	0.017	0.135	9.01
		1-2	0.395	0.148	0.366	0.011	0.059	6.42
		2-3	0.355	0.142	0.352	0.010	0.056	6.40
		3-4	0.210	0.145	0.326	0.010	0.057	6.48
		4-5	0.059	0.138	0.326	0.010	0.057	6.78
		5-7	0.014	0.141	0.315	0.012	0.067	6.62
		7-9	0.213	0.134	0.303	0.011	0.061	6.59
		9-11	0.338	0.364	1.003	0.009	0.058	7.21
		11-13	0.382	0.497	1.254	0.014	0.059	5.05
		15-17	2.366	0.127	0.283	0.012	0.062	6.29
		21-23	0.893	0.507	1.334	--	--	--
		27-29	0.596	0.218	0.531	0.014	0.074	6.15
10/28/2009	M	0-1	1.701	0.375	1.118	0.014	0.177	14.65
		1-2	0.976	0.530	1.946	0.017	0.143	9.75
		2-3	0.842	0.333	1.066	0.010	0.097	11.35
		3-4	0.776	0.338	0.939	0.010	0.075	8.70
		4-5	0.717	0.745	1.940	0.009	0.074	9.93
		5-7	0.689	0.254	0.629	0.008	0.064	9.34
		7-9	0.680	0.179	0.465	0.008	0.099	14.27
		9-11	0.862	0.246	0.702	0.010	0.091	10.94
		11-13	1.770	0.281	0.713	0.011	0.223	23.55
		15-17	3.714	0.257	0.600	0.014	0.303	26.19
		21-23	1.738	0.229	0.850	0.009	0.154	18.98

27-29	1.111	0.009	0.259	0.007	0.083	13.15
31-33	2.424	0.086	0.253	0.006	0.136	25.24
37-39	3.640	0.397	1.221	0.015	0.340	26.77
41-43	1.330	0.074	0.219	0.007	0.080	13.83
47-49	1.636	0.015	0.140	0.011	0.080	8.24
51-53	2.887	0.073	0.242	0.013	0.122	10.65

--no data

REFERENCES

Almroth, E., Tengberg, A., Andersson, J.H., Pakhomova, S., Hall, P.O., 2009. Effects of resuspension on benthic fluxes of oxygen, nutrients, dissolved inorganic carbon, iron and manganese in the Gulf of Finland, Baltic Sea. Continental Shelf Research 29, 807-818.

Andersen, K., Kjær, T., Revsbech, N., 2001. An oxygen insensitive microsensor for nitrous oxide. Sensors and Actuators B: Chemical 81, 42-48.

Archer, D., Devol, A., 1992. Benthic oxygen fluxes on the Washington shelf and slope: A comparison of in situ microelectrode and chamber flux measurements. Limnology and Oceanography 37, 614-629.

Aubinet, M., 2008. Eddy covariance CO2 flux measurements in nocturnal conditions: an analysis of the problem. Ecological Applications 18, 1368-1378.

Barth, J., Menge, B., Lubchenco, J., Chan, F., Bane, J., Kirincich, A., McManus, M., Nielsen, K., Pierce, S., Washburn, L., 2007. Delayed upwelling alters nearshore coastal ocean ecosystems in the northern California current. Proceedings of the National Academy of Sciences of the United States of America 104, 3719-3724.

Barth, J., Pierce, S., Castelao, R., 2005. Time-dependent, wind-driven flow over a shallow midshelf submarine bank. Journal of Geophysical Research 110.

Berg, P., 2008. Personal communication. Department of Environmental Sciences, University of Virginia, 291 McCormick Road, Charlottesville, VA 22904-4123, USA.

Berg, P., Glud, R., Hume, A., Stahl, H., Oguri, K., Meyer, V., Kitazato, H., 2009. Eddy correlation measurements of oxygen uptake in deep ocean sediments. Limnology and Oceanography-Methods 7, 576-584.

Berg, P., Huettel, M., 2008. Monitoring the seafloor using the noninvasive eddy correlation technique: Integrated Benthic Exchange Dynamics. Oceanography 21, 164-167.

Berg, P., Risgaard-Petersen, N., Rysgaard, S., 1998. Interpretation of measured concentration profiles in sediment pore water. Limnology and Oceanography 43, 1500-1510.

Berg, P., Roy, H., Janssen, F., Meyer, V., Jorgensen, B., Huettel, M., de Beer, D., 2003. Oxygen uptake by aquatic sediments measured with a novel non-invasive eddy-correlation technique. Marine Ecology Progress Series 261, 75-83.

Berg, P., Roy, H., Wiberg, P., 2007. Eddy correlation flux measurements: The sediment surface area that contributes to the flux. Limnology and Oceanography 52, 1672-1684.

Boehlert, G., Gill, A., 2010. Environmental and ecological effects of ocean renewable energy development; a current synthesis. Oceanography 23, 68-81.

Bograd, S., Castro, C., Di Lorenzo, E., Palacios, D., Bailey, H., Gilly, W., Chavez, F., 2008. Oxygen declines and the shoaling of the hypoxic boundary in the

California Current. Geophysical Research Letters 35.
Burdige, D., 2006. Geochemistry of Marine Sediments. Princeton University Press, Princeton.
Cai, W., Reimers, C., 1995. Benthic oxygen flux, bottom water oxygen concentration and core top organic carbon content in the deep northeast Pacific Ocean. Deep-Sea Research Part I-Oceanographic Research Papers 42, 1681-1699.
Cai, W., Sayles, F., 1996. Oxygen penetration depths and fluxes in marine sediments. Marine Chemistry 52, 123-131.
Chan, F., Barth, J., Lubchenco, J., Kirincich, A., Weeks, H., Peterson, W., Menge, B., 2008. Emergence of anoxia in the California Current large marine ecosystem. Science 319, 920-920.
Connolly, T., Hickey, B., Geier, S., Cochlan, W., 2010. Processes influencing seasonal hypoxia in the northern California Current System. Journal of Geophysical Research-Oceans 115.
Franke, U., Polerecky, L., Precht, E., Huettel, M., 2006. Wave tank study of particulate organic matter degradation in permeable sediments. Limnology and Oceanography 51, 1084-1096.
Glud, R., 2008. Oxygen dynamics of marine sediments. Marine Biology Research 4, 243-289.
Glud, R., Stahl, H., Berg, P., Wenzhofer, F., Oguri, K., Kitazato, H., 2009. In situ microscale variation in distribution and consumption of O-2: A case study from a deep ocean margin sediment (Sagami Bay, Japan). Limnology and Oceanography 54, 1-12.
Goring, D., Nikora, V., 2002. Despiking acoustic Doppler velocimeter data. Journal of Hydraulic Engineering 128, 117-126.
Graf, G., Schulz, R., Peinert, R., Meyer-Reill, L., 1983. Benthic response to sedimentation events during autumn to spring at a shallow-water station in the Western Kiel Bight. Marine Biology 77, 235-246.
Grantham, B., Chan, F., Nielsen, K., Fox, D., Barth, J., Huyer, A., Lubchenco, J., Menge, B., 2004. Upwelling-driven nearshore hypoxia signals ecosystem and oceanographic changes in the northeast Pacific. Nature 429, 749-754.
Hales, B., Karp-Boss, L., Perlin, A., Wheeler, P., 2006. Oxygen production and carbon sequestration in an upwelling coastal margin. Global Biogeochemical Cycles 20.
Hansen, J., Josefson, A., 2003. Accumulation of algal pigments and live planktonic diatoms in aphotic sediments during the spring bloom in the transition zone of the North and Baltic Seas. Marine Ecology Progress Series 248, 41-54.
Harley, C., Hughes, A., Hultgren, K., Miner, B., Sorte, C., Thornber, C., Rodriguez, L., Tomanek, L., Williams, S., 2006. The impacts of climate change in coastal marine systems. Ecology Letters 9, 228-241.
Hill, J., Wheeler, P., 2002. Organic carbon and nitrogen in the northern California current system: comparison of offshore, river plume, and coastally upwelled waters. Progress In Oceanography 53, 369-387.
Huettel, M., Røy, H., Precht, E., Ehrenhauss, S., 2003. Hydrodynamical impact on

biogeochemical processes in aquatic sediments. Hydrobiologia 494, 231-236.
Huettel, M., Webster, I., 2001. The benthic boundary layer: transport processes and biogeochemistry. Oxford University Press US.
Huettel, M., Ziebis, W., Forster, S., 1996. Flow-Induced Uptake of Particulate Matter in Permeable Sediments. Limnology and Oceanography 41, 309-322.
Huettel, M., Ziebis, W., Forster, S., Luther, G.W., 1998. Advective Transport Affecting Metal and Nutrient Distributions and Interfacial Fluxes in Permeable Sediments. Geochimica et Cosmochimica Acta 62, 613-631.
Ingram, R., 1971. Sieve analysis., in: Procedures in sedimentary petrology. Wiley Interscience, New York., pp. 49-67.
Jackson, J., Kirby, M., Berger, W., Bjorndal, K., Botsford, L., Bourque, B., Bradbury, R., Cooke, R., Erlandson, J., Estes, J., Hughes, T., Kidwell, S., Lange, C., Lenihan, H., Pandolfi, J., Peterson, C., Steneck, R., Tegner, M., Warner, R., 2001. Historical Overfishing and the Recent Collapse of Coastal Ecosystems. Science 293, 629-637.
Jahnke, R., Nelson, J., Marinelli, R., Eckman, J., 2000. Benthic flux of biogenic elements on the Southeastern US continental shelf: influence of pore water advective transport and benthic microalgae. Continental Shelf Research 20, 109-127.
Janssen, F., Faerber, P., Huettel, M., Meyer, V., Witte, U., 2005. Pore-Water Advection and Solute Fluxes in Permeable Marine Sediments (I): Calibration and Performance of the Novel Benthic Chamber System Sandy. Limnology and Oceanography 50, 768-778.
Janssen, F., Huettel, M., Witte, U., 2005. Pore-Water Advection and Solute Fluxes in Permeable Marine Sediments (II): Benthic Respiration at Three Sandy Sites with Different Permeabilities (German Bight, North Sea). Limnology and Oceanography 50, 779-792.
Keeling, R., Kortzinger, A., Gruber, N., 2010. Ocean Deoxygenation in a Warming World. Annual Review of Marine Science 2, 199-229.
Kirincich, A., Barth, J., Grantham, B., Menge, B., Lubchenco, J., 2005. Wind-driven inner-shelf circulation off central Oregon during summer. Journal of Geophysical Research 110.
Kuwae, T., Kamio, K., Inoue, T., Miyoshi, E., Uchiyama, Y., 2006. Oxygen exchange flux between sediment and water in an intertidal sandflat, measured in situ by the eddy-correlation method. Marine Ecology Progress Series 307, 59-68.
Lohse, L., Epping, E., Helder, W., van Raaphorst, W., 1996. Oxygen pore water profiles in continental shelf sediments of the North Sea:turbulent versus molecular diffusion. Marine Ecology Progress Series 145, 63-75.
McGinnis, D., Berg, P., Brand, A., Lorrai, C., Edmonds, T., Wuest, A., 2008. Measurements of eddy correlation oxygen fluxes in shallow freshwaters: Towards routine applications and analysis. Geophysical Research Letters 35.
Morse, J.W., Eldridge, P.M., 2007. A non-steady state diagenetic model for changes in sediment biogeochemistry in response to seasonally hypoxic/anoxic conditions in the "dead zone" of the Louisiana shelf. Marine Chemistry 106, 239-255.

Ozkan-Haller, T., 2008. Personal communication. College of Oceanic and Atmospheric Science, Oregon State University, 104 COAS Administration Building, Corvallis, OR 97331-5503.

Pauly, D., Christensen, V., Guenette, S., Pitcher, T., Sumaila, U., Walters, C., Watson, R., Zeller, D., 2002. Towards sustainability in world fisheries. Nature 418, 689-695.

Pierce, S., Barth, J., 2010. Cumulative wind stress: a data product for Oregon upwelling-related research [WWW Document]. URL http://damp.coas.oregonstate.edu/windstress/

Pinnegar, J., Polunin, N., Francour, P., Badalamenti, F., Chemello, R., Harmelin-Viven, M., Hereu, B., Milazzo, M., Zabala, M., D'Anna, G., Pipitone, C., 2000. Trophic cascades in benthic marine ecosystems: lessons for fisheries and protected-area management. Environmental Conservation 27, 179-200.

Precht, E., Huettel, M., 2003. Advective Pore-Water Exchange Driven by Surface Gravity Waves and Its Ecological Implications. Limnology and Oceanography 48, 1674-1684.

Precht, E., Ulrich, F., Polerecky, L., Huettel, M., 2004. Oxygen Dynamics in Permeable Sediments with Wave-Driven Pore Water Exchange. Limnology and Oceanography 49, 693-705.

Reimers, C., Glud, R., 2000. In situ chemical sensor measurements at the sediment-water interface, in: Varney, M. (Ed.), Chemical Sensors in Oceanography, Ocean Science and Technology. Gordon and Breach, Amsterdam, pp. 249-282.

Reimers, C., Jahnke, R., McCorkle, D., 1992. Carbon fluxes and burial rates over the continental slope and rise off central California with implications for the global carbon cycle. Global Biogeochemical Cycles 6, 199-224.

Reimers, C., McCann-Grosvenor, K., Sanders, R., Simpkin, J., 2010. BOXER: An eddy correlation lander for studies of Benthic OXygen Exchange Rates on continental shelves, in: Novel Sensors, Platforms, and Analytical Approaches in Biogeochemistry I. Presented at the Ocean Sciences 2010, Portland, OR.

Reimers, C., Smith, K., 1986. Reconciling measured and predicted fluxes of oxygen across the deep-sea sediment-water interface. Limnology and Oceanography 31, 305-318.

Reimers, C., Stecher, H., Taghon, G., Fuller, C., Huettel, M., Rusch, A., Ryckelynck, N., Wild, C., 2004. In situ measurements of advective solute transport in permeable shelf sands. Continental Shelf Research 24, 183-201.

Revsbech, N., 1989. An oxygen microsensor with a guard cathode. Limnology and Oceanography 34, 474-478.

Rocha, C., Forster, S., Koning, E., Epping, E., 2005. High-resolution permeability determination and two-dimensional porewater flow in sandy sediment. Limnology and Oceanography-Methods 3, 10-23.

Romsos, C., Goldfinger, C., Robison, R., Milstein, R., Chaytor, J., Wakefield, W., 2007. Development of a regional seafloor surficial geologic habitat map for the continental margins of Oregon and Washington, USA. In: Mapping the Seafloor for Habitat Characterization.

Rowe, G., Smith Jr., K., Clifford, C., 1976. Benthic-pelagic coupling in the New York Bight. American Society of Limnology and Oceanography.

Rowe, G., Theroux, R., Phoel, W., Quinby, H., Wilke, R., Koschoreck, D., Whitledge, T., Falkowski, P., Fray, C., 1988. Benthic carbon budgets for the continental shelf south of New England. Continental Shelf Research 8, 511-527.

Rusch, A., Huettel, M., Wild, C., Reimers, C., 2006. Benthic oxygen consumption and organic matter turnover in organic-poor, permeable shelf sands. Aquatic Microbial Ecology 12, 1-19.

Severmann, S., McManus, J., Berelson, W., Hammond, D., 2010. The continental shelf benthic iron flux and its isotope composition. Geochimica et Cosmochimica Acta 74, 3984-4004.

Strickland, J., Parsons, T., 1972. A Practical Handbook of Seawater Analysis, 2nd ed. Fisheries Research Board of Canada, Ottawa.

Tegner, M.J., Dayton, P.K., 2000. Ecosystem effects of fishing in kelp forest communities. ICES Journal of Marine Sciences 57, 579-589.

Tengberg, A., De Bovee, F., Hall, P., Berelson, W., Chadwick, D., Ciceri, G., Crassous, P., Devol, A., Emerson, S., Gage, J., Glud, R., Graziottini, F., Gundersen, J., Hammond, D., Helder, W., Hinga, K., Holby, O., Jahnke, R., Khripounoff, A., Lieberman, S., Nuppenau, V., Pfannkuche, O., Reimers, C., Rowe, G., Sahami, A., Sayles, F., Schurter, M., Smallman, D., Wehrli, B., De Wilde, P., 1995. Benthic chamber and profiling landers in oceanography -- A review of design, technical solutions and functioning. Progress In Oceanography 35, 253-294.

Verardo, D., Froelich, P., McIntyre, A., 1990. Determination of organic-carbon and nitrogen in marine-sediments using the Carlo-Erba NA 1500 analyzer. Deep-Sea Research Part A-Oceanographic Research Papers 37, 157-165.

Walsh, J., Rowe, G., Iverson, R., McRoy, C., 1981. Biological export of shelf carbon is a sink of the global CO2 cycle. Nature 291, 196-201.

Wetz, M., Hales, B., Wheeler, P., 2008. Degradation of phytoplankton-derived organic matter: Implications for carbon and nitrogen biogeochemistry in coastal ecosystems. Estuarine, Coastal and Shelf Science 77, 422-432.